

A more detailed and quantitative consideration of organized convection: Part III

Supercell thunderstorms and severe tornadoes

Best reference for this part is Bluestein's book, Vol. 2, Ch. 3

Miller Composite Sounding Types

Some background from Bluestein's book

U.S. Air force began forecasting based on upper-air observations in 1948 in response to a tornado hitting Tinker Air Force base near Oklahoma City

1952 The Severe Local Storms Forecasting unit of the Weather Bureau started to forecast severe weather

SELS moved to Kansas City and become National Severe Storms Forecasting Center in 1966. Later moved to Norman, Oklahoma

Four characteristics soundings associated with strong convection identified, developed by Col. R. Miller (in Air Force Manual)

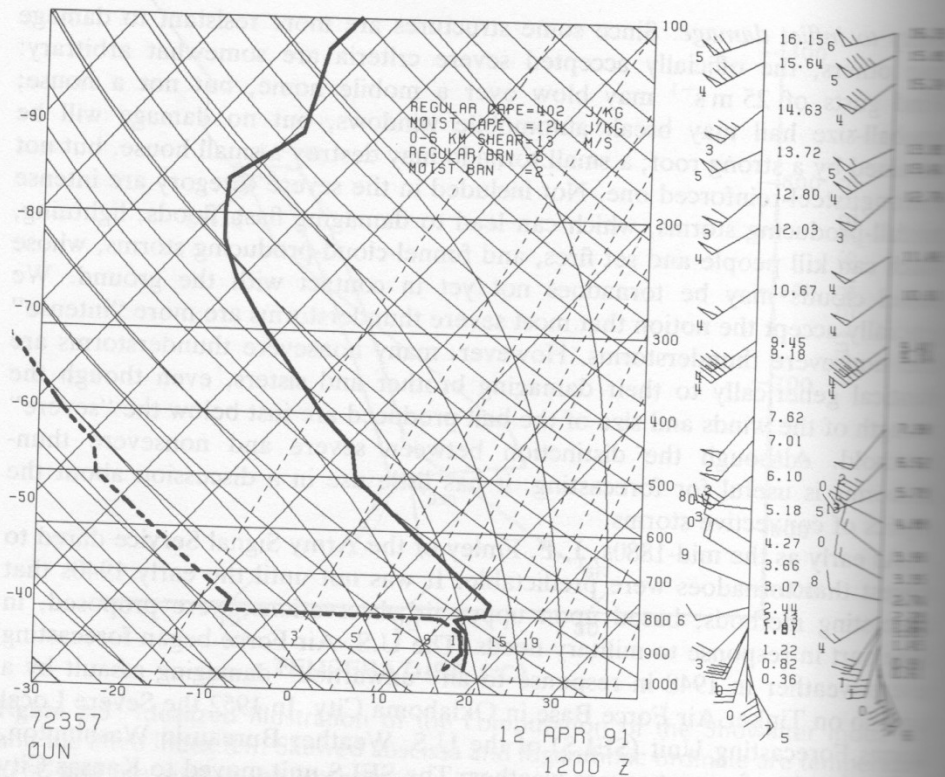


Figure 3.10 Example of a typical Miller “Type I” sounding in the United States. Sounding is at Norman, Oklahoma, at 1200 UTC, April 12, 1991 (0600 LST). Skewed abscissa and logarithmic ordinate are temperature ($^{\circ}\text{C}$) and pressure (mb), respectively. The plot of temperature and dew point are given by the thick solid and dashed lines, respectively. Winds plotted at the right; pennant = 25 m s^{-1} ; whole barb = 5 m s^{-1} ; half barb = 2.5 m s^{-1} . The moist air in the boundary layer (surface to 810 mb) comes from the Gulf of Mexico; the mixing ratio from the surface to 850 mb is nearly constant. The layer of low static stability above the moist layer comes from an elevated, deep, dry boundary layer over Mexico. The air above the Mexican layer (above 450 mb) comes from the western United States. The latter is separated from the former by a 50-mb deep stable layer. A stable layer, which in this case is an inversion, caps the moist layer around 800 mb. Several tornadic thunderstorms occurred in north-central Oklahoma later on in the day.

MILLER TYPE I

Well mixed, moist boundary layer of about 100-mb. High theta-e air.

Stable, dry inversion above low-level moist layer (cap)

Cold and very unstable aloft.

Directional shear.

The “loaded gun” sounding discussed earlier in reference to supercell thunderstorms

MILLER TYPE II

The tropical sounding

Deep moist layer up to at least seven km, so pretty close to moist adiabatic.

Little if any capping inversion

Possibility of widespread convection, but typically not too severe

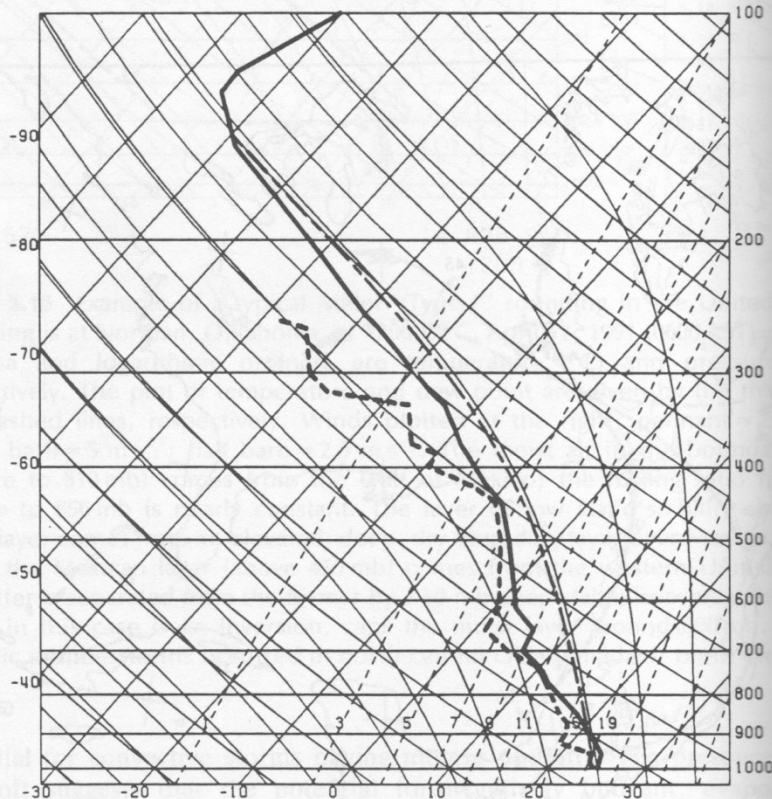


Figure 3.12 Example of a Miller "Type II" sounding in the United States. Skewed abscissa and logarithmic ordinate are temperature ($^{\circ}\text{C}$) and pressure (mb). Temperature (solid line); dew point (dashed line); moist-adiabat along which surface air parcel ascends (dot-dashed line). For Centerville, Alabama, 0000 UTC, August 17, 1985. This sounding was associated with a tornado outbreak and the remains of Hurricane Danny (from McCaul, 1987). (Courtesy of the American Meteorological Society)

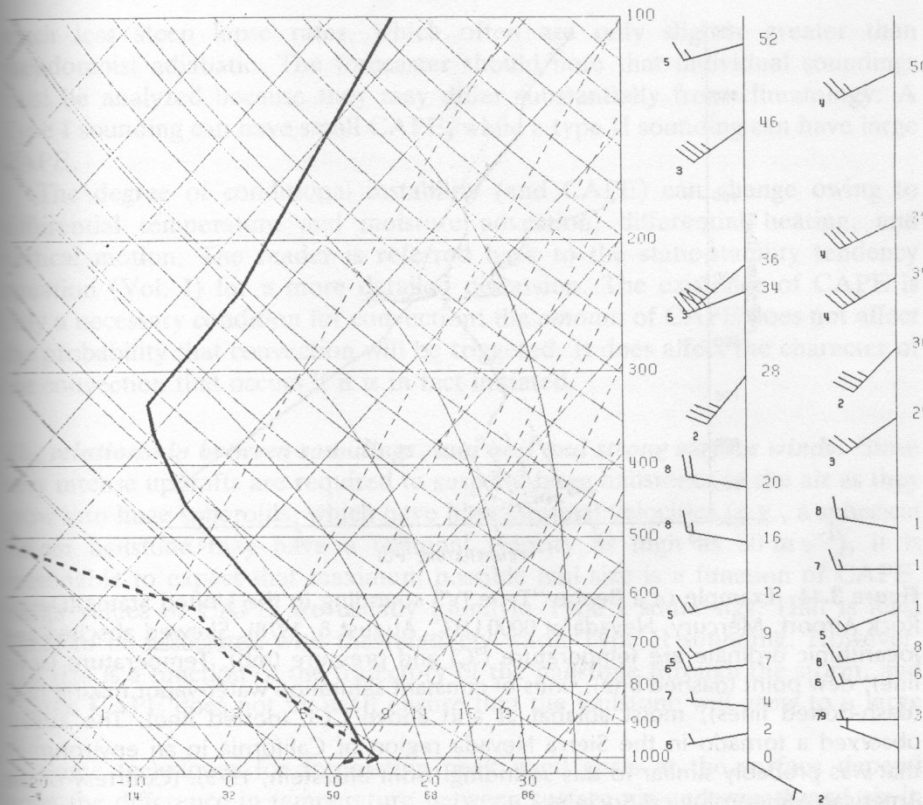


Figure 3.13 Example of a Miller “Type III” sounding in the United States. Sounding for Oakland, California, 1200 UTC, September 10, 1985. Skewed abscissa and logarithmic ordinate are temperature ($^{\circ}\text{C}$) and pressure (mb), respectively. The plot of temperature and dew point are given by the thick solid and dashed lines, respectively. Winds plotted at the right; whole barb = 5 m s^{-1} ; half barb = 2.5 m s^{-1} . A waterspout was reported over nearby San Francisco Bay near the time of this sounding. A cold upper-level low was situated over Northern California. Note the relatively cold -25°C temperature at 500 mb, and the relatively low tropopause (about 325 mb); also note the weak vertical wind shear and light land breeze at the surface from the southeast.

MILLER TYPE III

Similar to type II, except much colder (by 10-15 degrees C)

Found in cold core of upper-level cyclones and troughs.

“Cold air” sounding

MILLER TYPE IV

No low-level moist layer.

Relative humidity increase with height in lower troposphere

High surface temperature with a deep, well mixed boundary layer that is nearly dry adiabatic.

The “inverted V” profile .

Produced when dry continental tropical air overlaid by cold, moist polar air.

Sounding for microbursts!

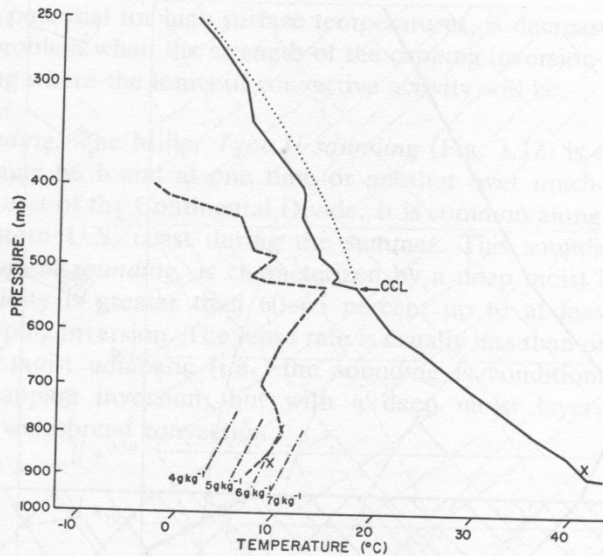


Figure 3.14 Example of a Beebe “Type IV” sounding in the United States (Desert Rock Airport, Mercury, Nevada at 0000 UTC, August 8, 1978). Skewed abscissa and logarithmic ordinate are temperature ($^{\circ}\text{C}$) and pressure (mb). Temperature (solid line); dew point (dashed line); lines of constant saturation water-vapor mixing ratio (dash-dotted lines); moist adiabat at and above CCL (dotted line). The author observed a tornado in the Sierra Nevada region of California in an environment that was probably similar to this sounding (from Bluestein, 1979). (Courtesy of the American Meteorological Society)

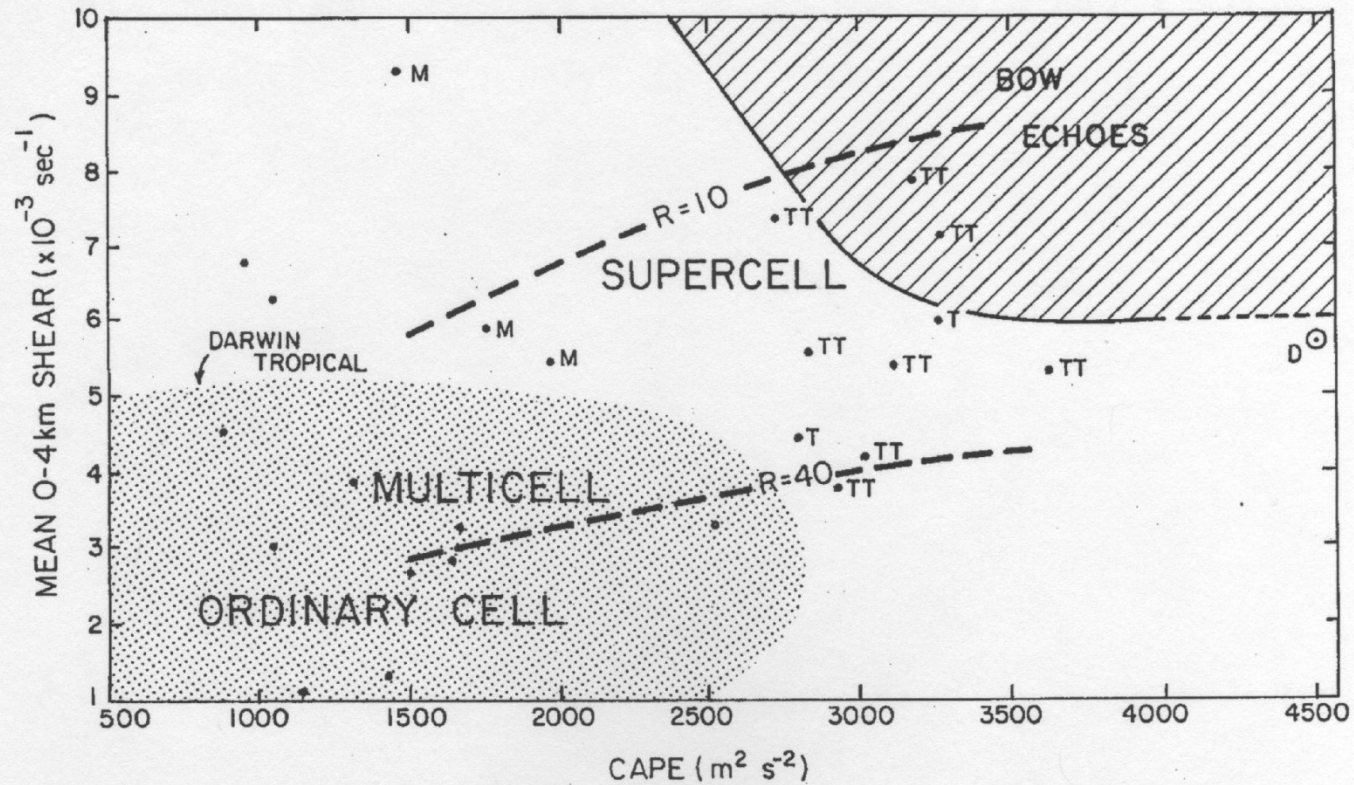
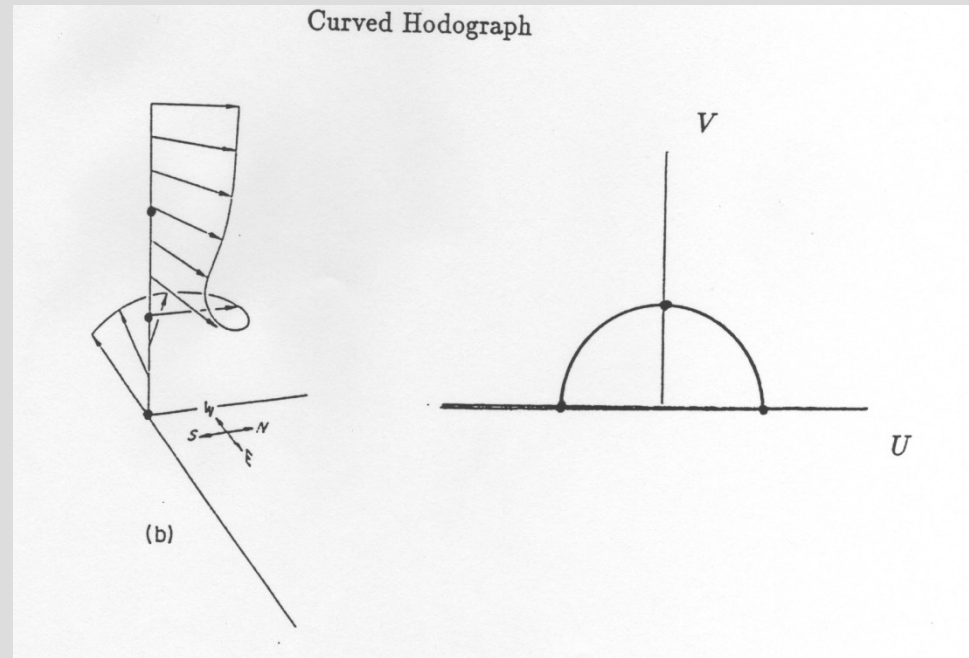
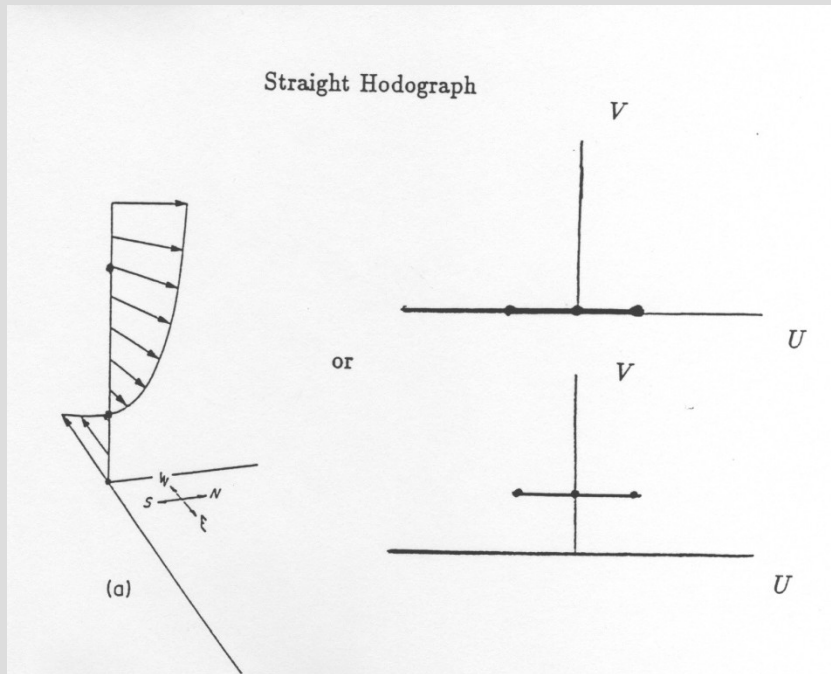


Figure 7.1: Types of convective elements as a function of mean vertical wind shear in the lowest 4 km and CAPE (from Rasmussen and Wilhelmson 1983). *M* represents a storm with a mesocyclone but no tornado, *T* a storm with one tornado, *TT* a storm with more than one tornado and an unmarked dot a storm without a mesocyclone. *D* represents mean conditions for derechos using data from Johns and Hirt (1987) and Johns et al. (1990). The heavy dashed lines indicate values of bulk Richardson number 10 and 40 (from Weisman and Klemp 1982, 1984, 1986). The shaded region indicates the approximate range of conditions found near Darwin, Australia, during the active and break monsoon periods (from Keenan and Carbone 1992). The hatched region indicates the range of conditions for bow echoes from Weisman 1993.

Unidirectional Shear vs. Directional Shear on Hodograph



In particular, observations show that a pronounced turning of the low-level shear vector is commonly found in proximity to supercell storms, especially those that produce tornadoes (e.g., Maddox 1976). This unique feature of midlatitude soundings can be expressed in terms of the *helicity* (H) of the environmental flow, where

$$H \equiv \boldsymbol{\omega} \cdot \mathbf{v},$$

3-D vort.
3-D velocity

and $\boldsymbol{\omega} = \nabla \times \mathbf{v}$. The importance of H for supercells or convection with strong rotation can be seen by considering the momentum equations in the form (following Lilly 1986)

$$\frac{\partial \mathbf{v}}{\partial t} + \mathbf{v} \cdot \nabla \mathbf{v} + \nabla \pi - b\mathbf{k} = 0, \quad (7.5)$$

Only vertical comp.

where $\pi \equiv (p - \bar{p})/\bar{\rho}$, $b = g(\theta_v - \bar{\theta}_v)/\bar{\theta}_v$ and overbar denotes a mean value. The advection term can be rewritten using the following identity:

$$\mathbf{v} \cdot \nabla \mathbf{v} = \nabla \frac{V^2}{2} + (\nabla \times \mathbf{v}) \times \mathbf{v}.$$

For purely helical flows $\boldsymbol{\omega}$ and \mathbf{v} are parallel. Then,

$$\mathbf{v} \cdot \nabla \mathbf{v} = \nabla \frac{V^2}{2}$$

and taking the curl of (7.5) yields

$$\frac{\partial \boldsymbol{\omega}}{\partial t} = \nabla b \times \mathbf{k}. \quad (7.6)$$

Since the RHS of (7.6) has no vertical component, vertically aligned helical flows can be long-lived and steady. In application, it is the storm-relative helicity of the environmental flow that is important (Davies-Jones 1984):

$$H = (\mathbf{v} - \mathbf{c}) \cdot \nabla \times \mathbf{v}, \quad (7.7)$$

where \mathbf{c} is the storm motion vector. Since the synoptic-scale flow is nearly horizontal, $(\mathbf{v} - \mathbf{c}) \cdot \nabla \times \mathbf{v} \approx \mathbf{k} \cdot (\mathbf{v} - \mathbf{c}) \times d\mathbf{v}/dz$, and therefore H is proportional to the area on a hodograph (Davies-Jones 1984).

In particular,

Vertical wind shear!

$$H(\mathbf{c}) = - \int_0^h \mathbf{k} \cdot (\mathbf{v} - \mathbf{c}) \times \frac{d\mathbf{v}}{dz} dz . \quad (7.8)$$

The integral in (7.8) is equivalent to twice the signed area swept out by the storm-relative wind vector between 0 and h (usually 3 km) on a hodograph (Fig. 7.3).

To estimate the storm motion vector (\mathbf{c}) in operational practice (e.g. from a morning sounding), consider pressure-weighted mean wind in lowest 5-6 km. In strong clockwise turning hodograph, add 5-10 m s⁻¹ to the right of the mean wind.

	<u>H (m² s⁻²)</u>
weak tornadoes	150-299
strong tornadoes	300-449
violent tornadoes	\gtrsim 450

$$H(\mathbf{c}) = - \int_0^h \mathbf{k} \cdot (\mathbf{v} - \mathbf{c}) \times \frac{d\mathbf{v}}{dz} dz . \quad (7.8)$$

The integral in (7.8) is equivalent to twice the signed area swept out by the storm-relative wind vector between 0 and h (usually 3 km) on a hodograph (Fig. 7.3).

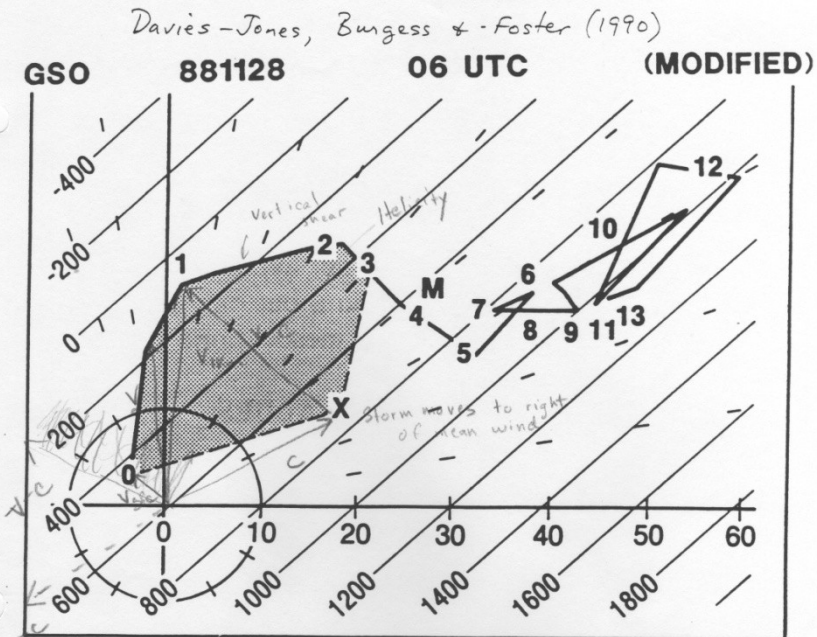


Fig. 7.3 *Hodograph for Raleigh, NC tornado environment (Nov 28, 1988). The 00 UTC sounding at Greensboro has been modified slightly by backing the winds 10° in the lowest 1.5 km to reflect conditions believed to exist in the tornado environment. Speed circles are every $10 m s^{-1}$ with dashed lines every 10° . Numbers along hodograph curve denote height AGL in km. Large X and M mark observed storm motion and mean wind between surface and 200 mb. The s-r helicity in the lowest 3 km is minus twice the shaded area (which is negative because the s-r wind turns clockwise with height). Straight lines parallel to 0-3 km shear vector are contours of helicity for this hodograph as a function of storm motion, i.e., the location of X. For observed storm motion of 240° at $20 m s^{-1}$, the helicity was $719 m^2 s^{-2}$ for the modified and $615 m^2 s^{-2}$ for the unmodified hodograph.*

Dynamics of supercell thunderstorm formation

Has mainly to do with dynamic pressure effects and tilting of horizontal vorticity in an environment of high (rotational) vertical shear, assuming you have the requisite thermodynamic conditions present.

Vorticity Equation

Synoptic and **Mesoscale** contributions

$$\frac{\partial \zeta_a}{\partial t} = \vec{V} \bullet \nabla \zeta_a - \omega \frac{\partial \zeta_a}{\partial p} - \left[\frac{\partial \omega}{\partial x} \frac{\partial v}{\partial p} - \frac{\partial \omega}{\partial y} \frac{\partial u}{\partial p} \right] + \zeta_a \frac{\partial \omega}{\partial p} + \left[\frac{\partial F_y}{\partial x} - \frac{\partial F_x}{\partial y} \right]$$

A B C D E F

A = local time rate of change term

B = Horizontal vorticity advection (PVA or NVA)


C = Vertical vorticity advection

D = Tilting of vorticity in the horizontal to the vertical

E = Vortex stretching (Diabatic heating or terrain changes)

F = Friction

Simplified equations of motion for convection on mesoscale

	<u>Full equation</u>		<u>Linearize, Boussinesq approx.</u>
U momentum	$\frac{Du}{Dt} = -\frac{1}{\rho} \frac{\partial p}{\partial x}$		$\frac{Du}{Dt} = -\frac{1}{\rho} \frac{\partial p'}{\partial x}$
V momentum	$\frac{Dv}{Dt} = -\frac{1}{\rho} \frac{\partial p}{\partial y}$		$\frac{Dv}{Dt} = -\frac{1}{\rho} \frac{\partial p'}{\partial y}$
W momentum	$\frac{Dw}{Dt} = -\frac{1}{\rho} \frac{\partial p}{\partial z} - g$		$\frac{Dw}{Dt} = -\frac{1}{\rho} \frac{\partial p'}{\partial z} + B$

IMPORTANT ASIDE: Absolutely no Coriolis effects here! So any rotations in supercell storms due ONLY to mesoscale dynamics—NOT the synoptic scale!

$$B = -\frac{\rho'}{\rho} g \quad \text{Buoyancy}$$

Differentiate u and v momentum equations with respect to x and y, respectively, then add together..

Add w momentum equation, differentiated with respect to z and assuming constant mean density, to get a **divergence equation**:

$$\frac{D}{Dt}(\nabla \bullet \bar{\mathbf{v}}) + \frac{1}{\rho} \nabla^2 p' = \left[\left(\frac{\partial u}{\partial x} \right)^2 + \left(\frac{\partial v}{\partial y} \right)^2 + \left(\frac{\partial w}{\partial z} \right)^2 + 2 \frac{\partial u}{\partial y} \frac{\partial v}{\partial x} + 2 \frac{\partial u}{\partial z} \frac{\partial w}{\partial x} + 2 \frac{\partial v}{\partial z} \frac{\partial w}{\partial y} \right] + \frac{\partial B}{\partial z}$$

Invoking a shallow water assumption, our first term on LHS vanishes because:

$$\nabla \bullet \bar{\mathbf{v}} = \frac{\partial u}{\partial x} + \frac{\partial v}{\partial y} + \frac{\partial w}{\partial z} = 0$$

Linearize about the following state:

$$u = \bar{u}(z) + u'(x, y, z, t)$$

$$v = \bar{v}(z) + v'(x, y, z, t)$$

$$w = w'(x, y, z, t)$$

Assume a linearly varying mean vertical wind profile of u and v, for simplicity.

Laplacian equation for pressure perturbation = **dynamic pressure + buoyancy**

$$\frac{1}{\rho} \nabla^2 p' = - \left[\left(\frac{\partial u'}{\partial x} \right)^2 + \left(\frac{\partial v'}{\partial y} \right)^2 + \left(\frac{\partial w'}{\partial z} \right)^2 + 2 \left(\frac{\partial u'}{\partial y} \frac{\partial v'}{\partial x} + \frac{\partial u'}{\partial z} \frac{\partial w'}{\partial x} + \frac{\partial v'}{\partial z} \frac{\partial w'}{\partial y} + \frac{\partial \bar{u}}{\partial z} \frac{\partial w'}{\partial x} + \frac{\partial \bar{v}}{\partial z} \frac{\partial w'}{\partial y} \right) \right] + \frac{\partial B}{\partial z}$$

$$p' = p'_{dyn} + p'_B = p'_{dynL} + p'_{dynNL} + p'_B$$

Linear dynamic contribution: Interaction of environmental shear with updraft vertical velocity (i.e. rotation of horizontal environmental vorticity into vertical)

$$\nabla^2 p'_{dynL} \propto - \left[\frac{\partial \bar{u}}{\partial z} \frac{\partial w'}{\partial x} + \frac{\partial \bar{v}}{\partial z} \frac{\partial w'}{\partial y} \right] = - \frac{\partial \bar{\mathbf{v}}_H}{\partial z} \cdot \nabla_H w'$$

Non-linear dynamic contributions: Fluid extension terms and shear terms

$$\nabla^2 p'_{dynNL} \propto - \left[\left(\frac{\partial u'}{\partial x} \right)^2 + \left(\frac{\partial v'}{\partial y} \right)^2 + \left(\frac{\partial w'}{\partial z} \right)^2 + 2 \left(\frac{\partial u'}{\partial y} \frac{\partial v'}{\partial x} + \frac{\partial u'}{\partial z} \frac{\partial w'}{\partial x} + \frac{\partial v'}{\partial z} \frac{\partial w'}{\partial y} \right) \right]$$

Fluid extension

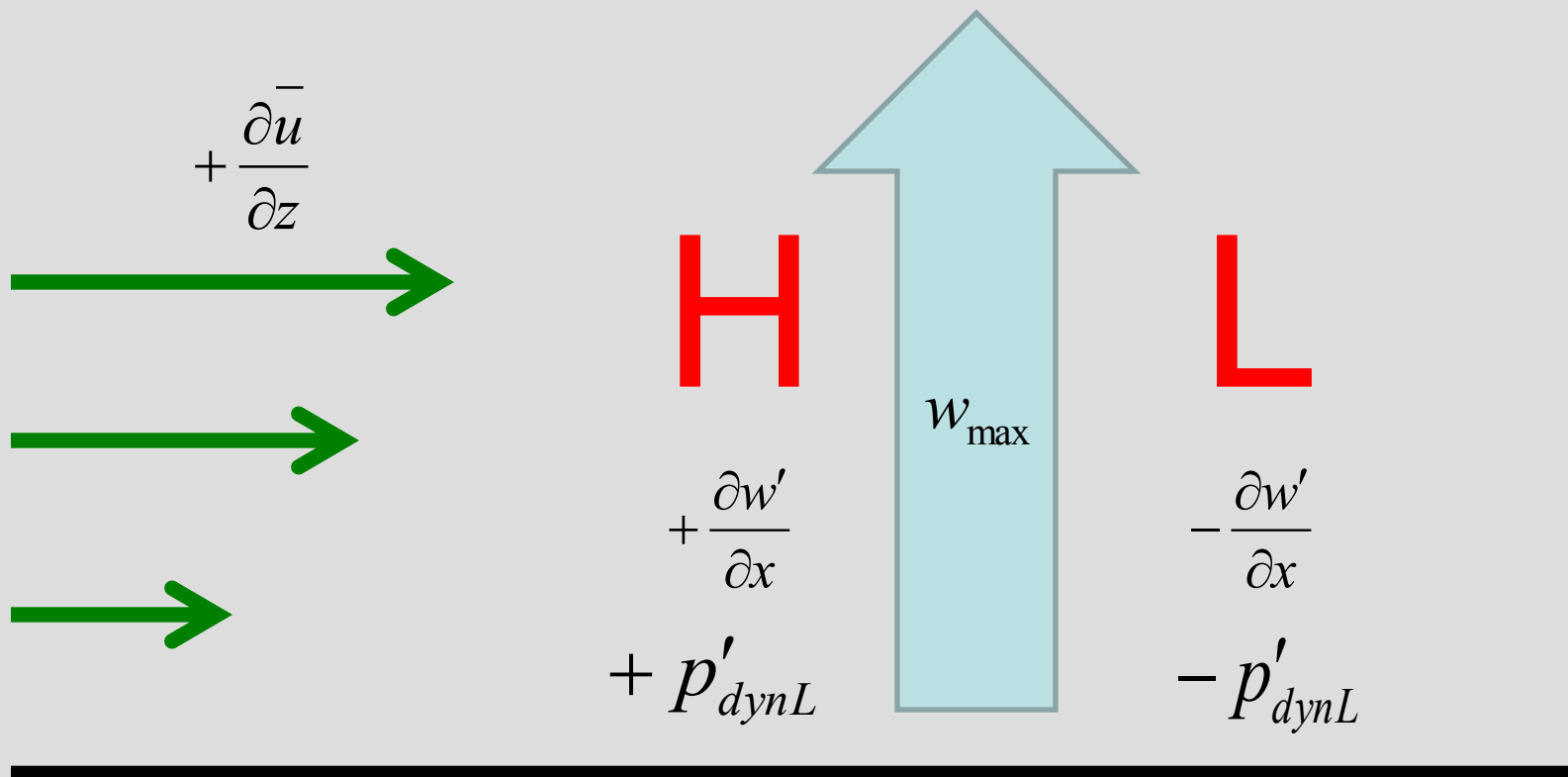
Shear

Contributions to dynamic pressure by linear dynamics

Since a Laplacian tends to change the sign of the variable on which it operates:

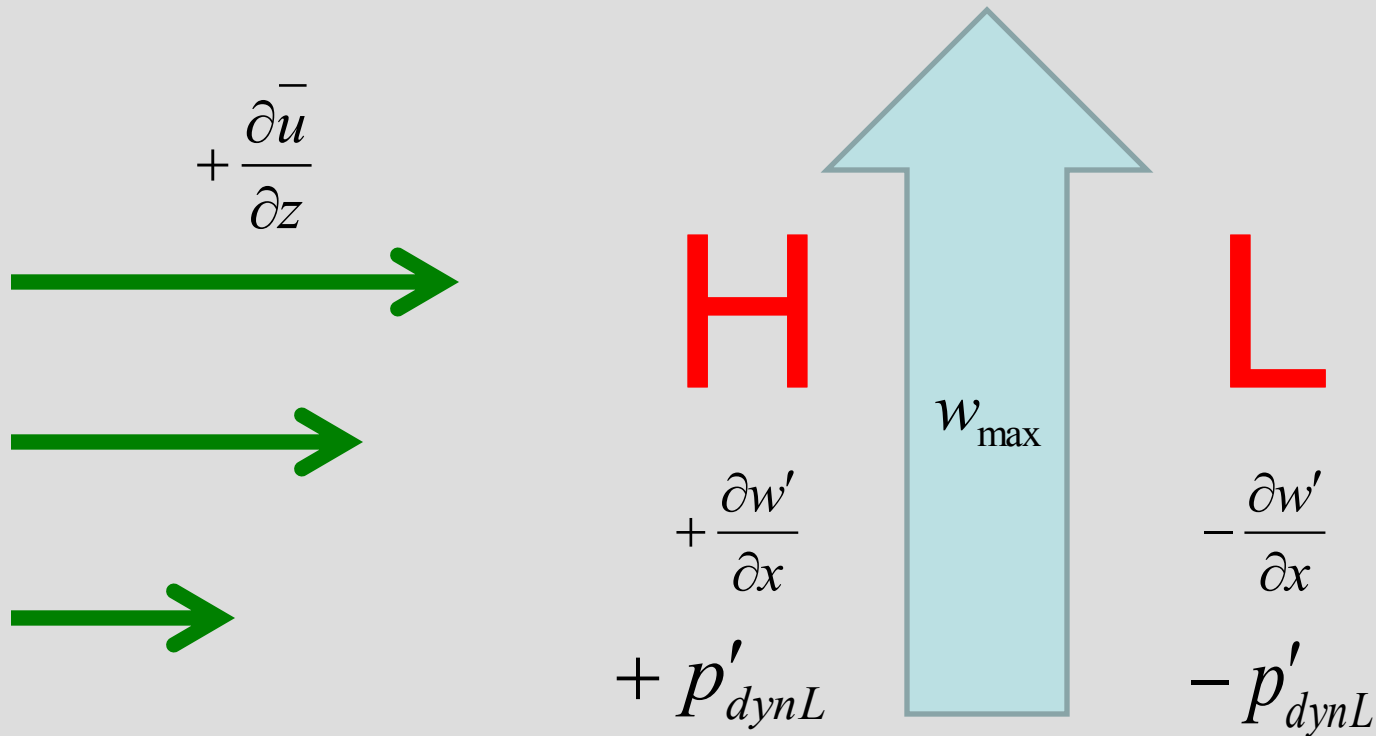
$$p'_{dynL} \propto \frac{\partial \bar{v}_H}{\partial z} \cdot \nabla_H w'$$

For an updraft in an environment of positive unidirectional zonal shear,
 Positive perturbation pressure on upshear side of updraft
 Negative perturbation pressure on downshear side of updraft

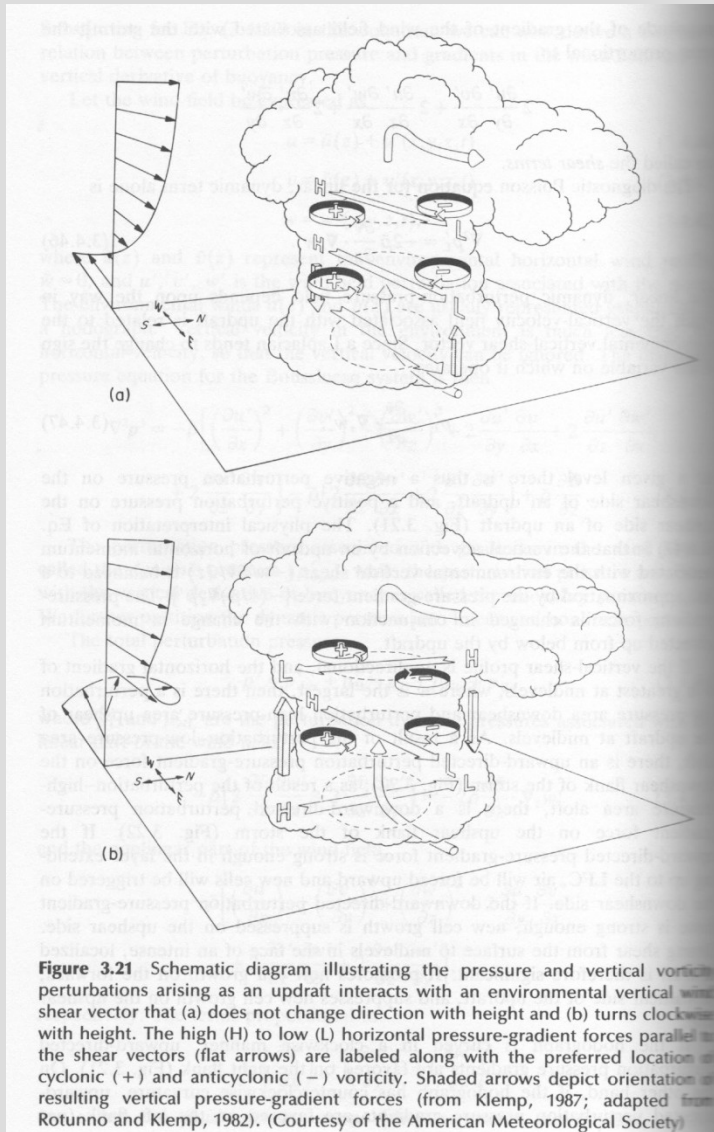


$$p'_{dynL} \propto \frac{\partial \bar{v}_H}{\partial z} \cdot \nabla_H w'$$

Physical interpretation: Vertical advection by an updraft of horizontal momentum associated with environmental shear is balanced by pressure gradient force.



Effects of linear pressure perturbation terms



Unidirectional shear

For a maximum updraft velocity in mid-levels, perturbation high pressure upshear, low pressure downshear. **Helps promote new cell growth downwind of the updraft in front of the storm.**

Directional (clockwise) shear

Upward directed pressure gradients are favored on more on the right flank of the storm. Opposite for counterclockwise shear.

Almost always a clockwise rotating shear profile for supercell thunderstorms in United States.

Contribution to pressure perturbation by non-linear dynamics

Shearing terms:

$$\nabla^2 p'_{dynNLshear} \propto -2 \left(\frac{\partial u'}{\partial y} \frac{\partial v'}{\partial x} + \frac{\partial u'}{\partial z} \frac{\partial w'}{\partial x} + \frac{\partial v'}{\partial z} \frac{\partial w'}{\partial y} \right)$$

Can express with deformation and vorticity terms in all directions:

$$= -\frac{1}{2} \left[\left(\frac{\partial v'}{\partial x} + \frac{\partial u'}{\partial y} \right)^2 - \left(\frac{\partial v'}{\partial x} - \frac{\partial u'}{\partial y} \right)^2 + \left(\frac{\partial u'}{\partial z} + \frac{\partial w'}{\partial x} \right)^2 - \left(\frac{\partial u'}{\partial z} - \frac{\partial w'}{\partial x} \right)^2 + \left(\frac{\partial w'}{\partial y} + \frac{\partial v'}{\partial z} \right)^2 - \left(\frac{\partial w'}{\partial y} - \frac{\partial v'}{\partial z} \right)^2 \right]$$

Shearing terms:

$$\nabla^2 p'_{dynNLshear} \propto -2 \left(\frac{\partial u'}{\partial y} \frac{\partial v'}{\partial x} + \frac{\partial u'}{\partial z} \frac{\partial w'}{\partial x} + \frac{\partial v'}{\partial z} \frac{\partial w'}{\partial y} \right)$$

Can express with deformation and vorticity terms in all directions:

$$= -\frac{1}{2} \left[\left(\frac{\partial v'}{\partial x} + \frac{\partial u'}{\partial y} \right)^2 - \left(\frac{\partial v'}{\partial x} - \frac{\partial u'}{\partial y} \right)^2 + \left(\frac{\partial u'}{\partial z} + \frac{\partial w'}{\partial x} \right)^2 - \left(\frac{\partial u'}{\partial z} - \frac{\partial w'}{\partial x} \right)^2 + \left(\frac{\partial w'}{\partial y} + \frac{\partial v'}{\partial z} \right)^2 - \left(\frac{\partial w'}{\partial y} - \frac{\partial v'}{\partial z} \right)^2 \right]$$

Consider tilting of unidirectional shear by an updraft, such that all deformation terms and horizontal vorticity terms (i.e. crossed out terms) are zero. **All that is left is vertical vorticity.**

$$\nabla^2 p'_{dynNLshear} \propto \left(\frac{\partial v'}{\partial x} - \frac{\partial u'}{\partial y} \right)^2 = \zeta'^2$$

$$p'_{dynNLshear} \propto -\zeta'^2$$

Again, sign changes with Laplacian inversion

Result: Non-linear shearing terms produce low perturbation pressure in the vicinity of mid-level anticyclonic and cyclonic vorticity induced by the updraft.

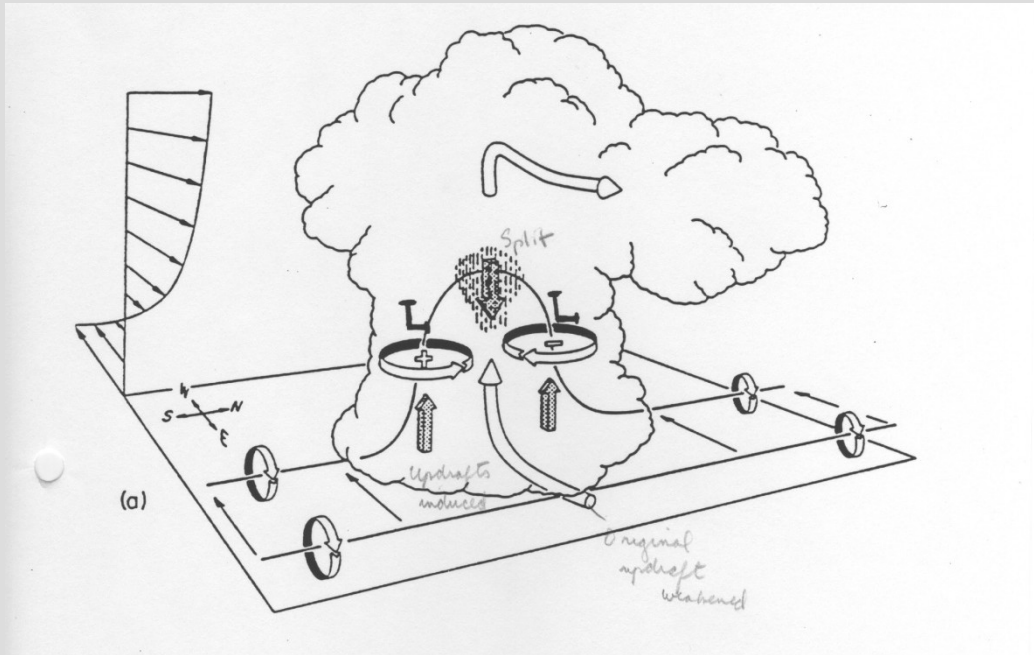
Effect of non-linear pressure perturbation terms (shearing)

In unidirectional shear

Have formation of mid-level vortices at storm flanks. Results from tilting of horizontal vorticity of the environment by updrafts results in perturbation low pressure.

This DOES NOT depend on the direction of rotation!

The upward directed pressure gradient at storm flanks will tend to enhance updrafts at the sides of the storm.



Storm splitting process

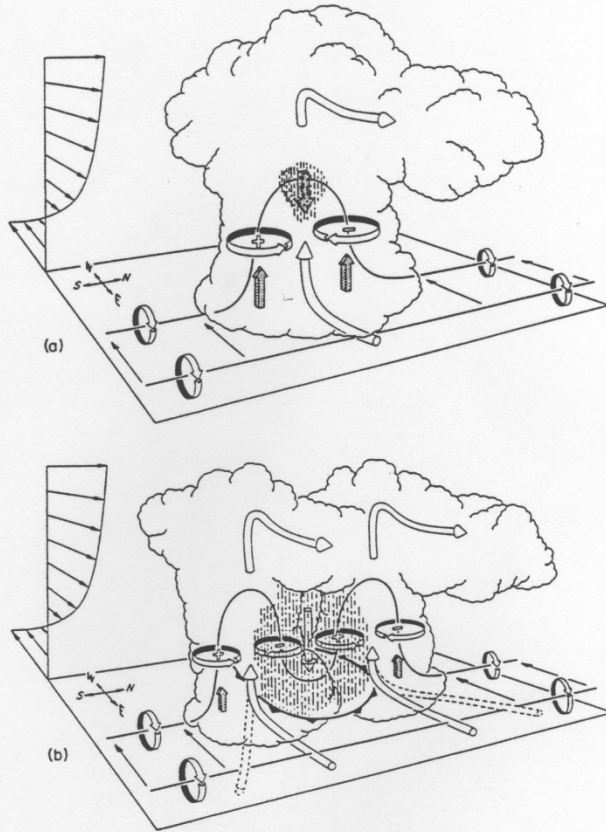


Figure 46. Schematic depicting how a typical vortex tube contained within (westerly) environmental shear is deformed as it interacts with a convective cell (viewed from the southeast). Cylindrical arrows show the direction of cloud- relative airflow, and heavy solid lines represent vortex lines with the sense of rotation indicated by circular arrows. Shaded arrows represent the forcing influences that promote new updraft and downdraft growth. Vertical dashed lines denote regions of precipitation. (a) Initial stage: Vortex tube loops into the vertical as it is swept into the updraft. (b) Splitting stage: Downdraft forming between the splitting updraft cell tilts vortex tubes downward, producing two vortex pairs. The barbed line at the surface marks the boundary of the cold air spreading out beneath the storm (from Klemp, 1987).

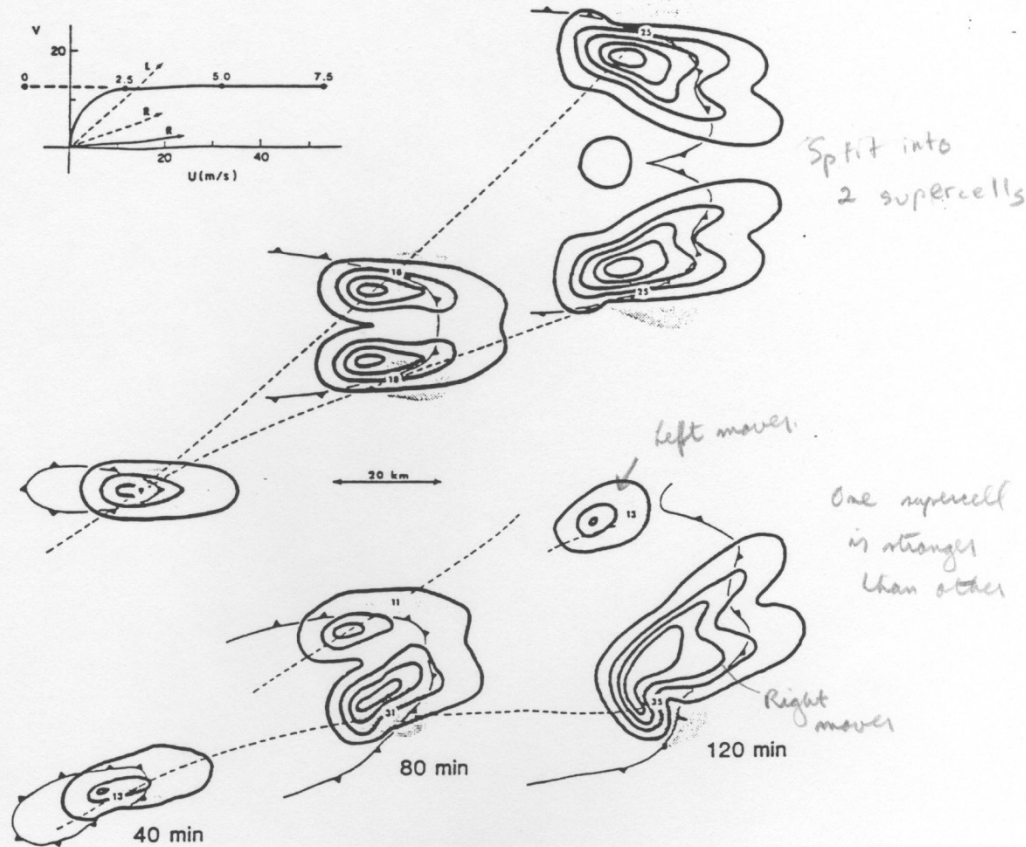
A downdraft in the center of the storm starts to weaken the updraft. Strongest vertical motion becomes more favored at right and left flanks.

The downdraft splits the storm into two:

Right mover: cyclonically rotating on the right flank

Left mover: anticyclonically rotating on the left flank.

The aforementioned linear perturbation pressure effects will favor the development of the right mover in an environment with clockwise rotating shear.



UNIDIRECTIONAL
SHEAR: Left and
right movers
equally favored

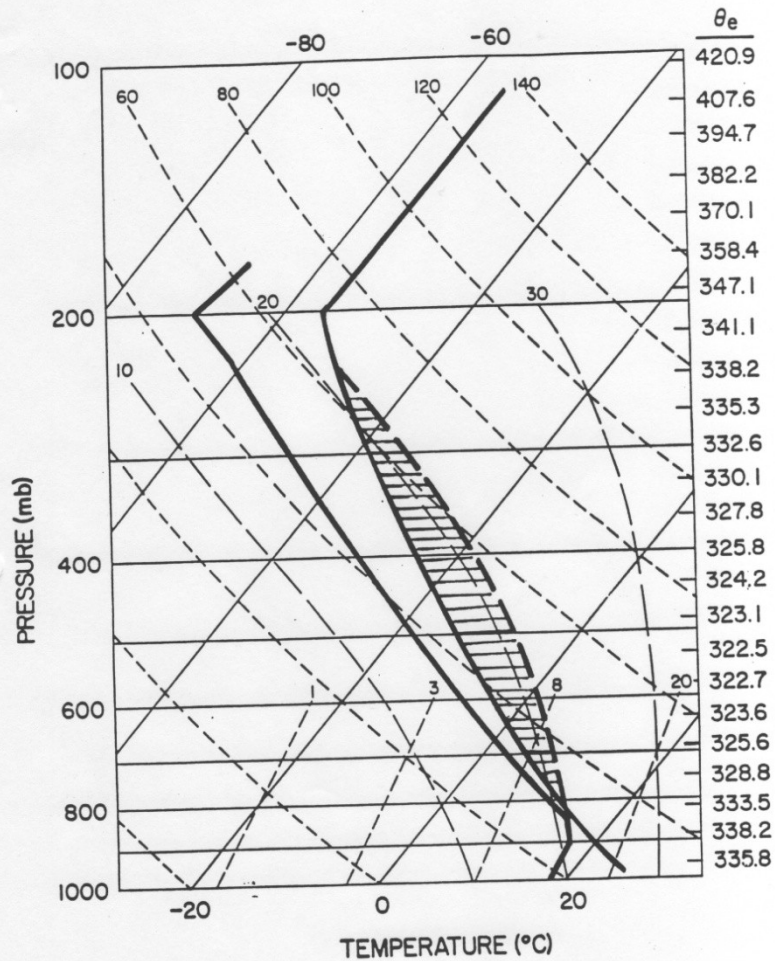
CLOCKWISE
ROTATING SHEAR
PROFILE: Favors
right mover

Figure 6 Plan views of numerically simulated thunderstorm structures at 40, 80, and 120 min for two environmental wind profiles (displayed at upper left) having wind shear between the surface and 7.5 km. The storm system in the lower portion of the figure evolves in response to the wind profile in which S turns clockwise with height between the ground and 2.5 km (heavy solid line in wind plot), while the upper system develops when S is unidirectional (same wind profile except following the heavy dashed line below 2.5 km). The plan views depict the low-level (1.8 km) rainwater field (similar to radar reflectivity) contoured at 2 g kg^{-1} intervals, the midlevel (4.6 km) updraft (shaded regions), and the location of the surface cold-air outflow boundary (barbed lines). The maximum updraft velocity is labeled (in m s^{-1}) within each updraft at each time. The dashed lines track the path of each updraft center. Arrows in the wind plot indicate the supercell propagation velocities for the unidirectional (dashed) and turning (solid) wind shear profiles. (Adapted from Klemp & Weisman 1983.)

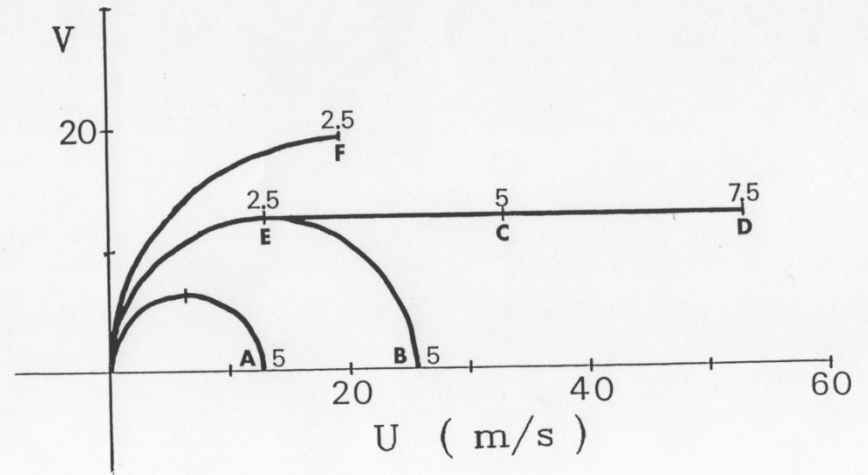
KLEMP-WILHELMSON
3-D NUMERICAL CLOUD MODEL

- * ***Compressible Equations of Motion***
- * ***Prognostic Variables: $u, v, w, t, p, q_v, q_c, q_r$***
- * ***Kessler-type parameterization for microphysics
(no ice)***
- * ***Subgrid scale turbulence parameterization
based on a turbulence energy equation***
- * ***Open lateral boundary conditions***
- * ***Storms initiated by a symmetric warm bubble
within a horizontally homogeneous environment,
characterized by specified vertical profiles of
wind, moisture, and temperature***

Constant idealized sounding



Vary wind shear profile (as seen in hodograph)



Bulk Richardson number (R)

Since storm strength is dependent on BOTH instability and shear, can define a bulk Richardson number (R).

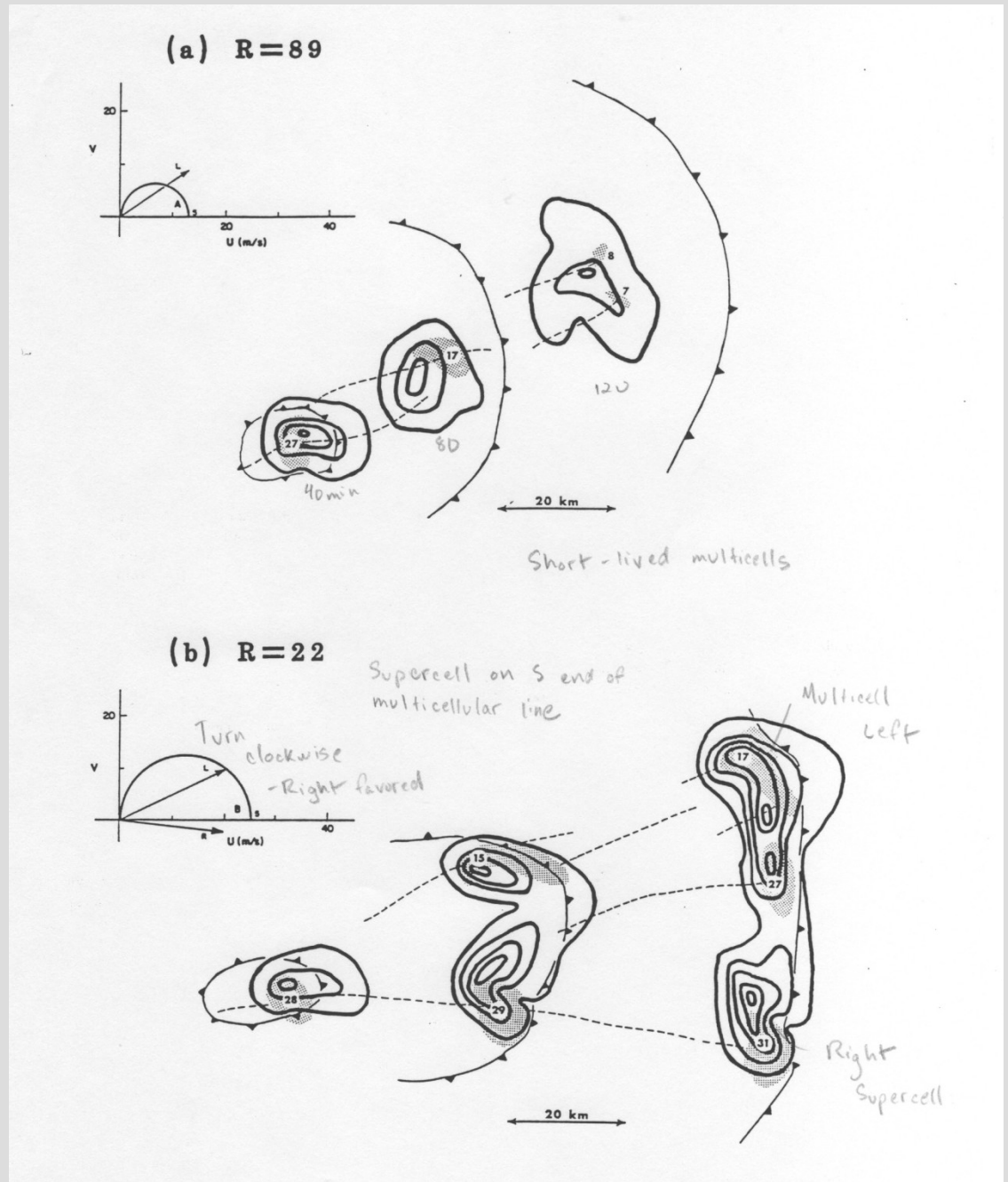
$$R = \text{CAPE}/S^2$$

$$S^2 = \frac{1}{2} (u_{6\text{km}} - u_{500\text{m}})^2$$

This measure gives some indication of the potential for organized convection.

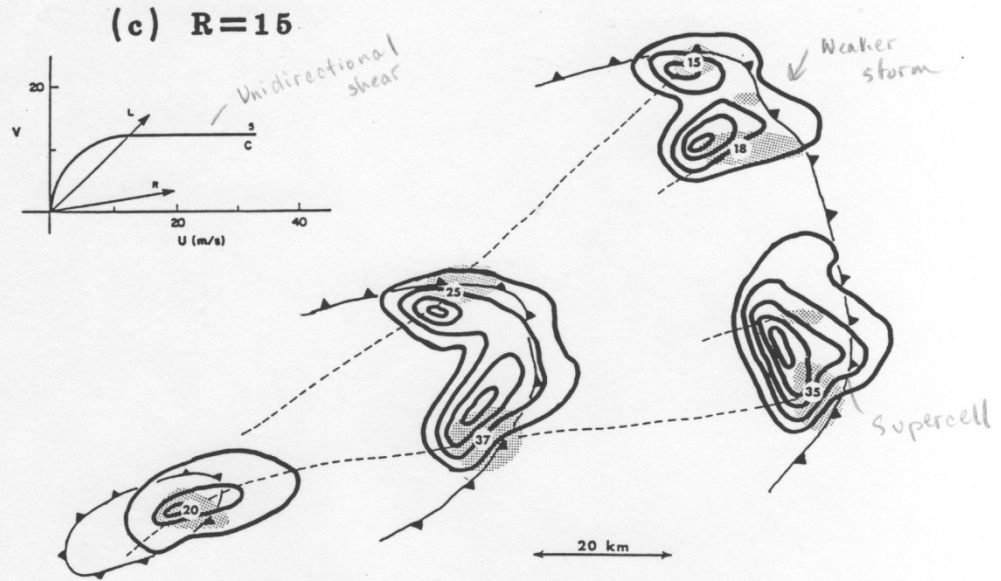
Supercell (tornadic) thunderstorms tend to form with $10 < R < 40$. So need some sort of optimal balance of CAPE vs. shear to get most intense kinds of thunderstorms.

CASE A

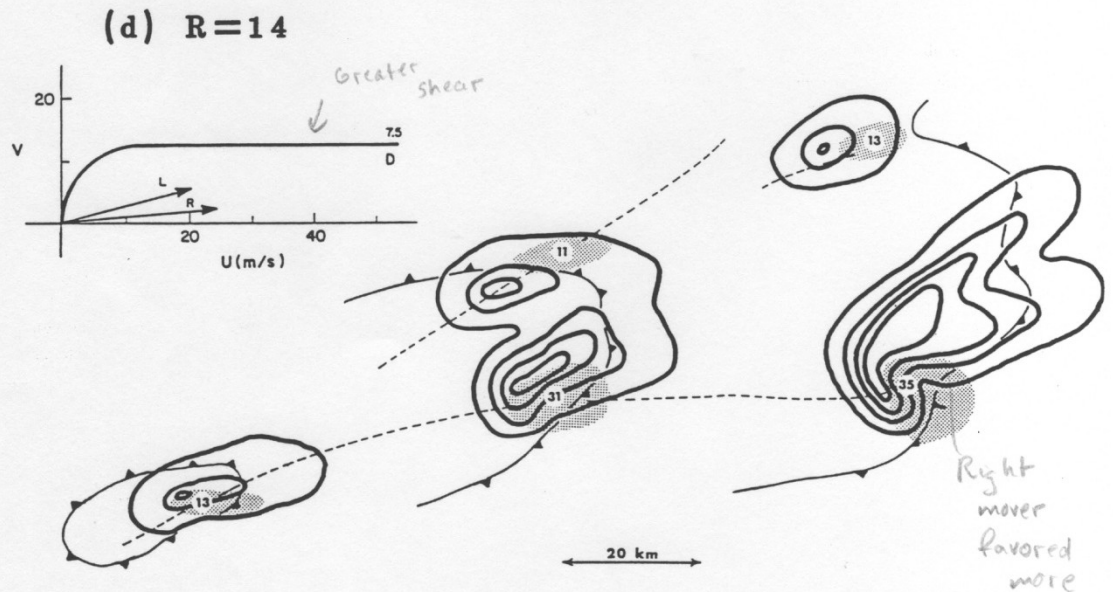


CASE B

CASE C

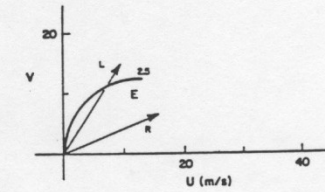


CASE D

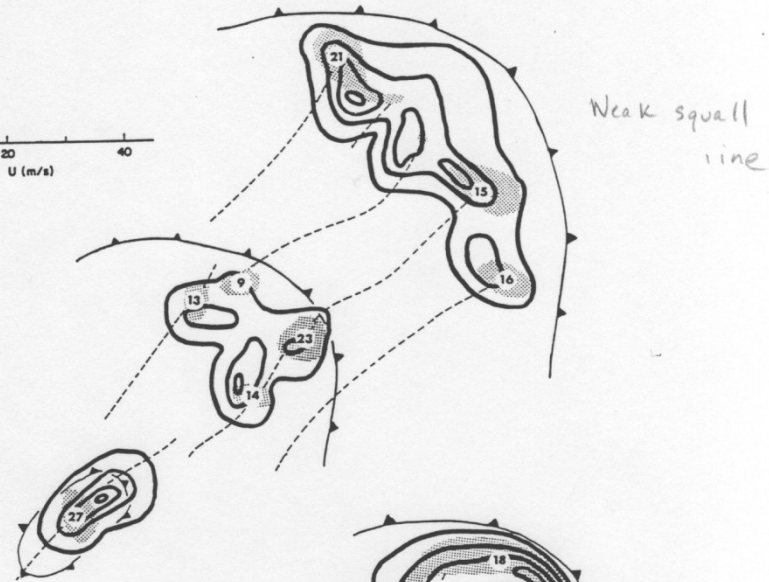


CASE E

(e) $R=34$

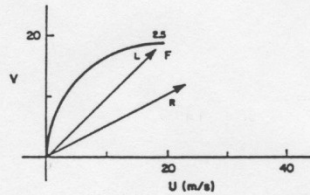


Shear truncated

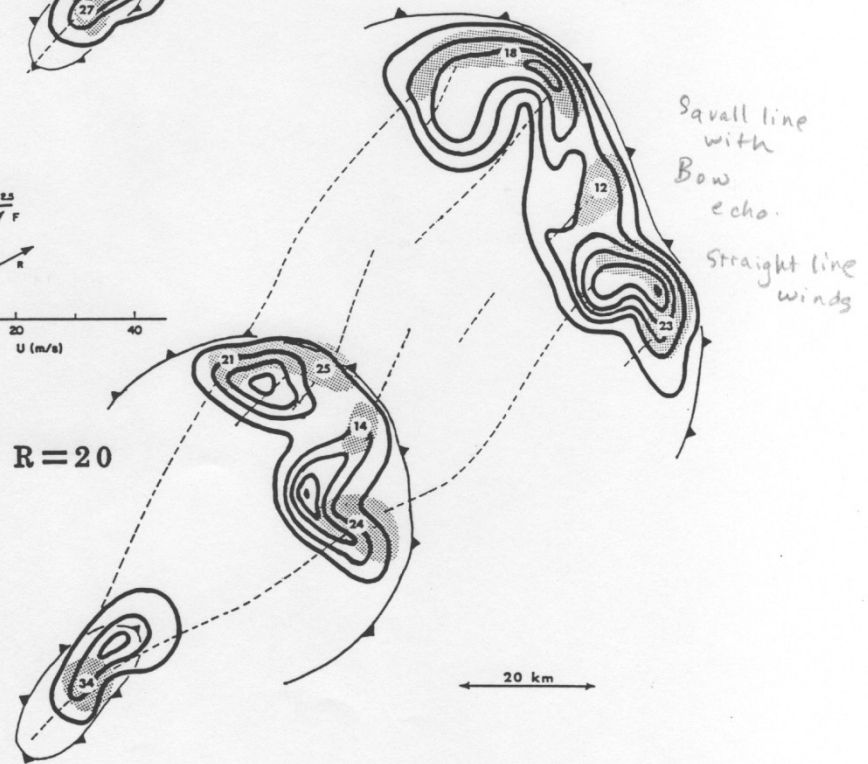


Weak squall line

CASE F



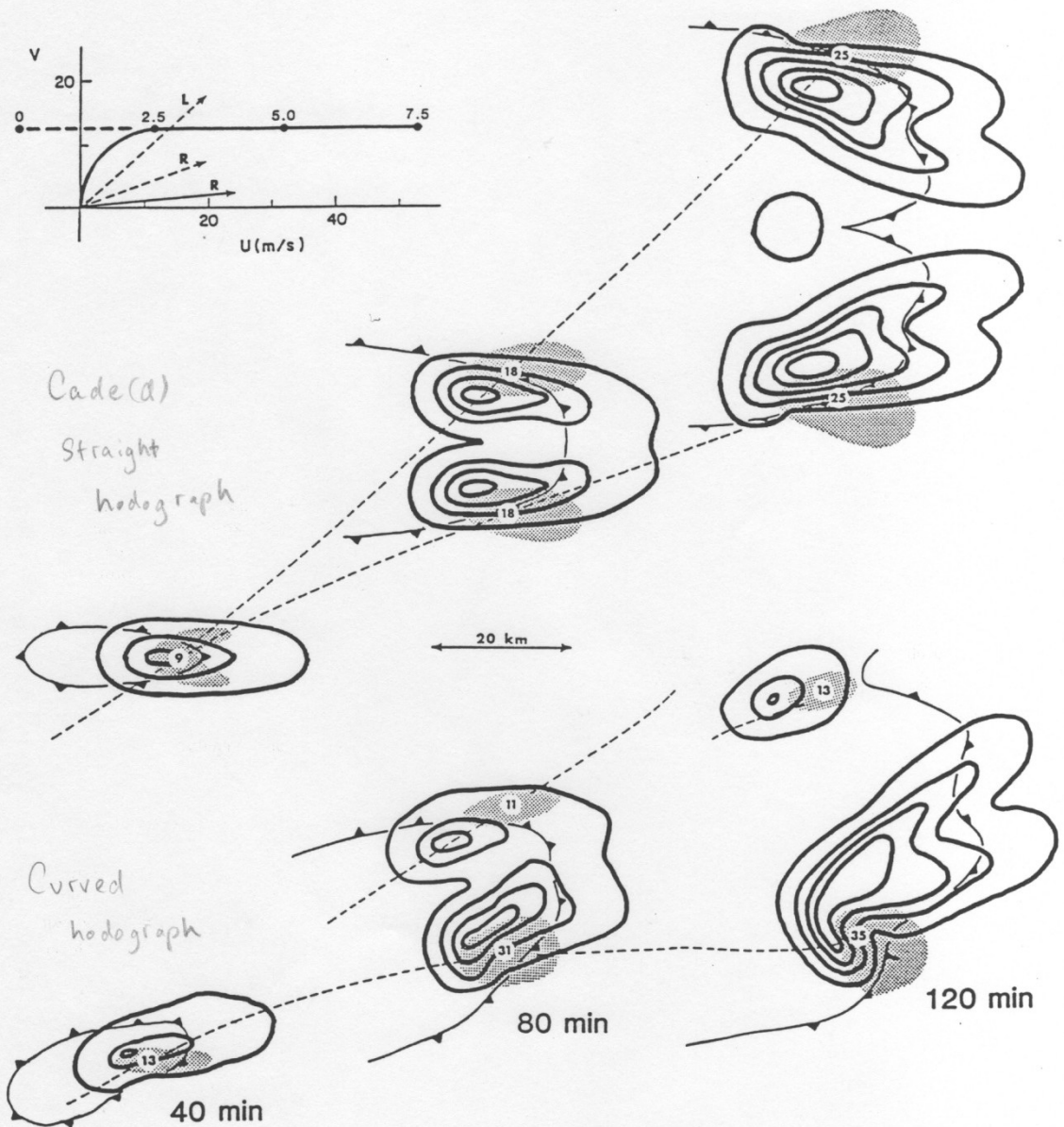
Same - but shear increased by 50% (f) $R=20$



Squall line with Bow echo. Straight line winds

CASE D

*Unidirectional shear
No helicity*

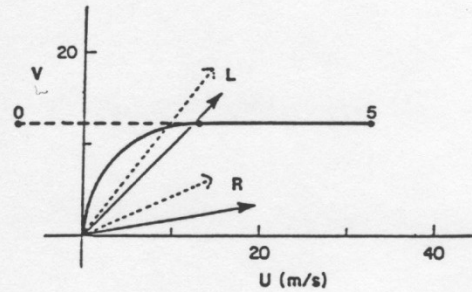


CASE D

*Directional shear
Has helicity*

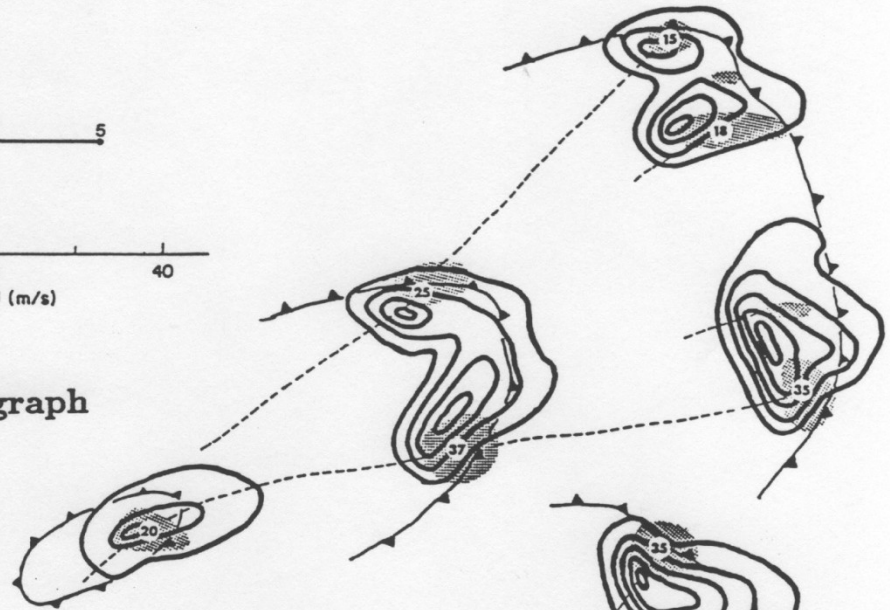
CASE C

Directional shear
Has helicity



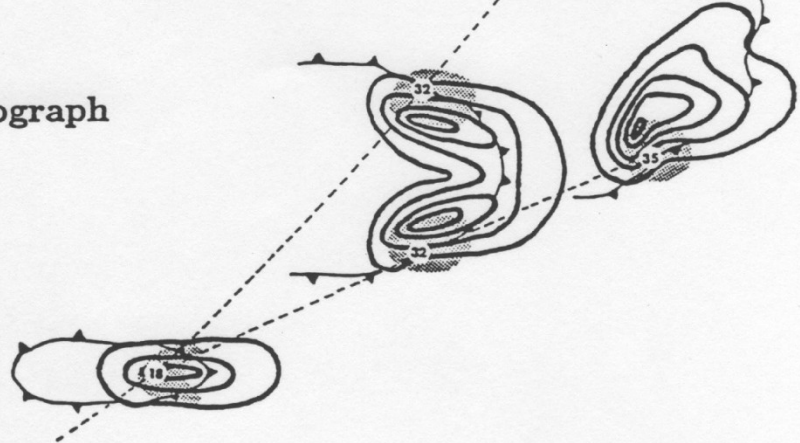
Curved Hodograph

$$R = 15$$



Straight Hodograph

$$R = 12$$



CASE C

Unidirectional shear
No helicity

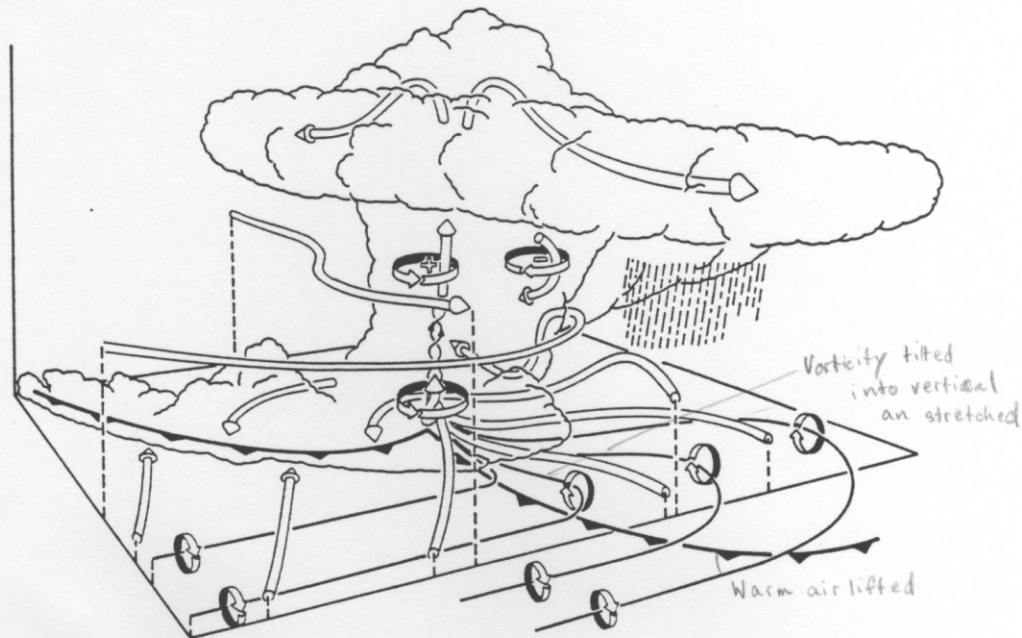


Figure 12 Three-dimensional schematic view of a numerically simulated supercell thunderstorm at a stage when the low-level rotation is intensifying. The storm is evolving in westerly environmental wind shear and is viewed from the southeast. The cylindrical arrows depict the flow in and around the storm. The thin lines show the low-level vortex lines, with the sense of rotation indicated by the circular-ribbon arrows. The heavy barbed line marks the boundary of the cold air beneath the storm.

Tornadogenesis preceded by the development of RFD and FFD. There is additional generation of horizontal vorticity along the edge of the cold pool in FFD.

A strong updraft tilts the horizontal vorticity into the vertical and stretches it

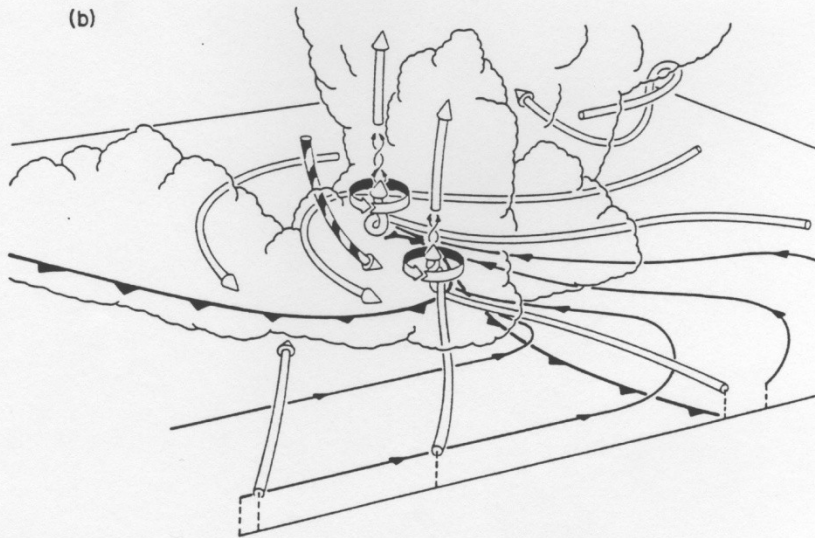
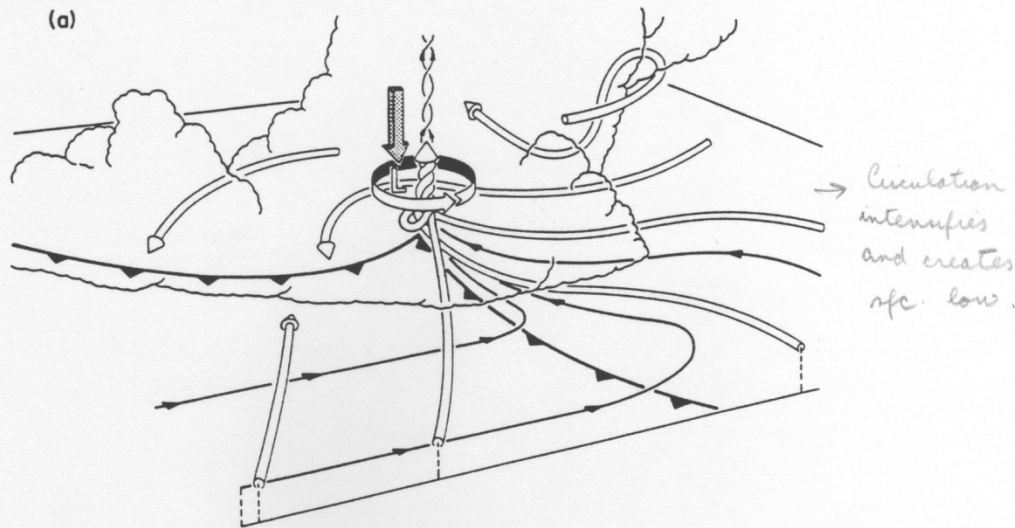


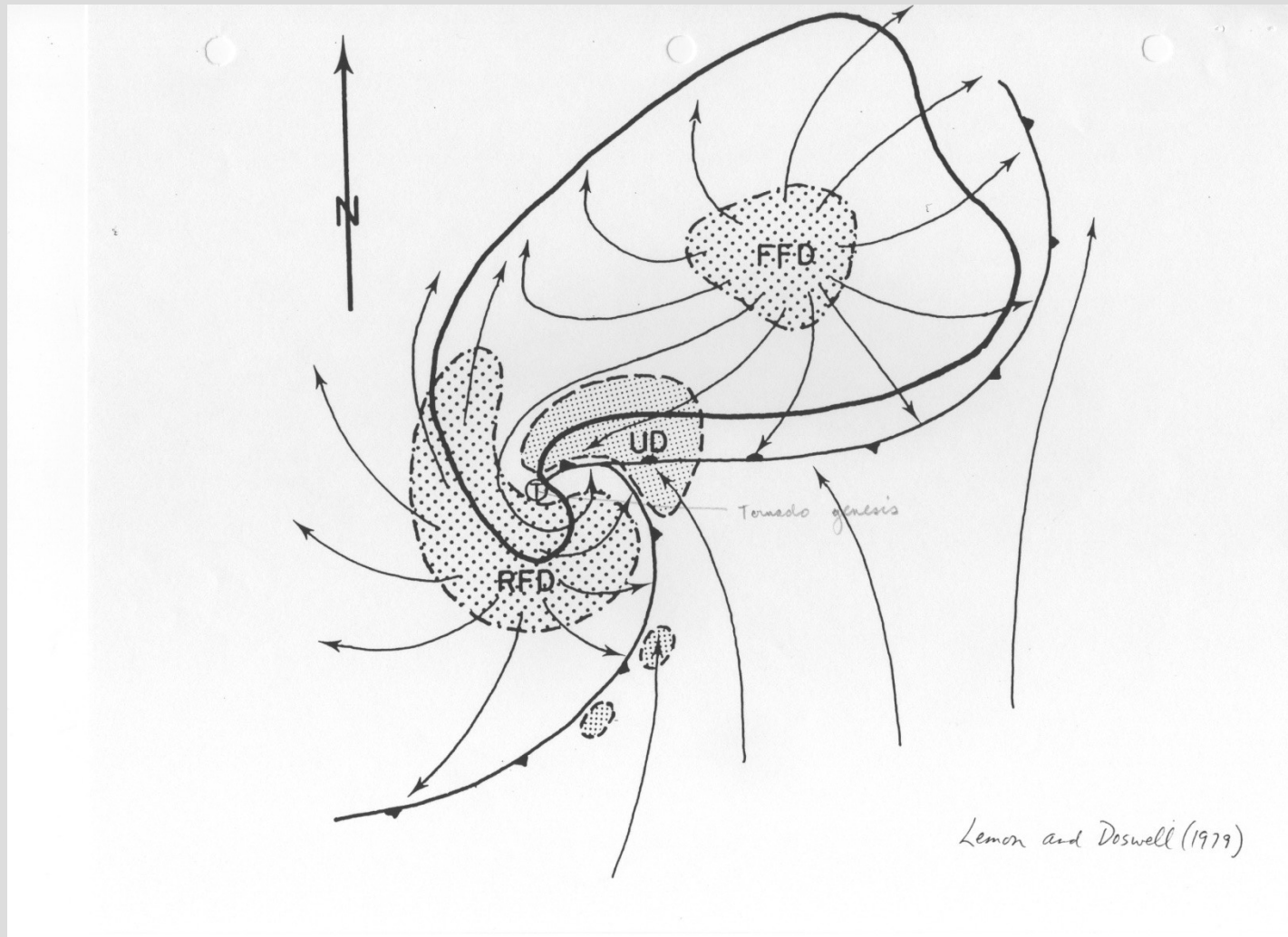
Figure 13 Expanded three-dimensional perspective, viewed from the southeast, of the low-level flow (a) at the time depicted in Figure 12, and (b) about 10 min later after the rear-flank downdraft has intensified. Features are drawn as described in Figure 12 except that the vector direction of vortex lines are indicated by arrows along the lines. The shaded arrow in (a) represents the rotationally induced vertical pressure gradient, and the striped arrow in (b) denotes the rear-flank downdraft.

The formation of the RFD is due to a downward directed perturbation pressure gradient due to the rapidly decreasing surface pressure.

The tornado forms in the updraft in front of the gust front of the RFD.

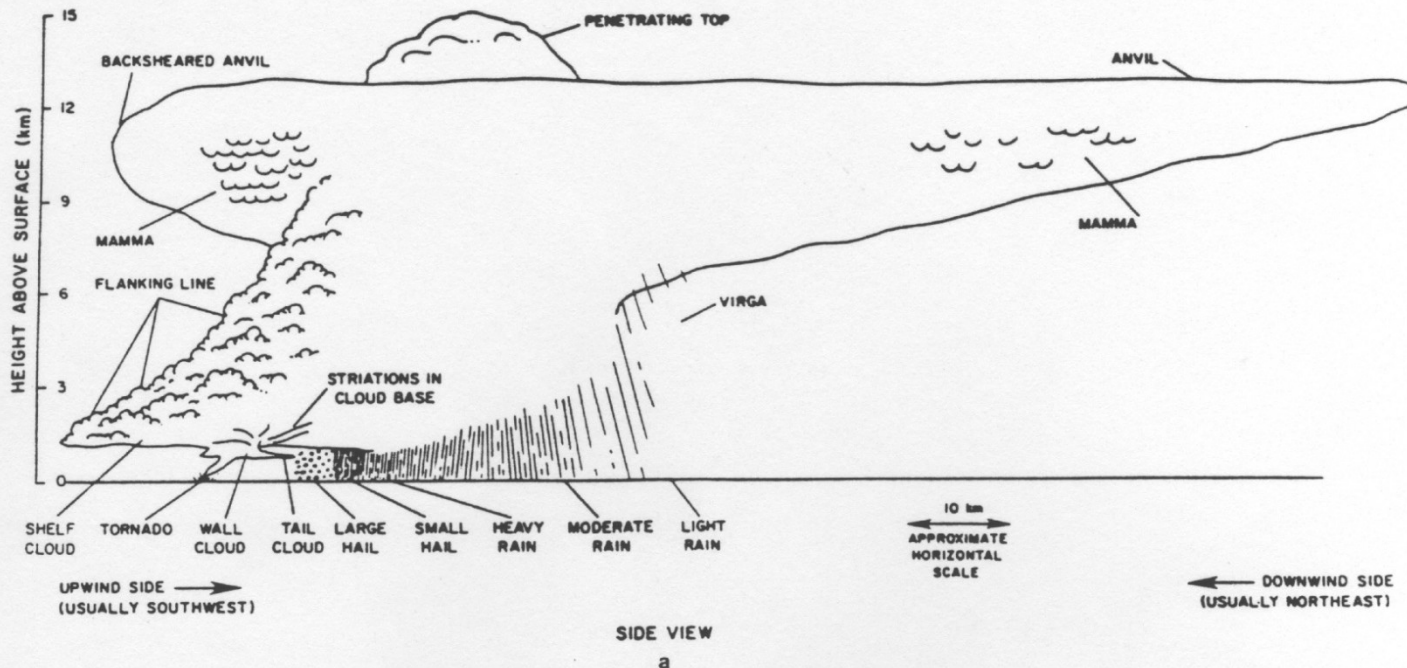
The exact trigger for what for the surface whirls that initiate tornado formation is still not well known.

Surface inflows and outflows and vertical motions in mature tornadic supercell



Classic supercell: Form in high directional shear, high CAPE environments

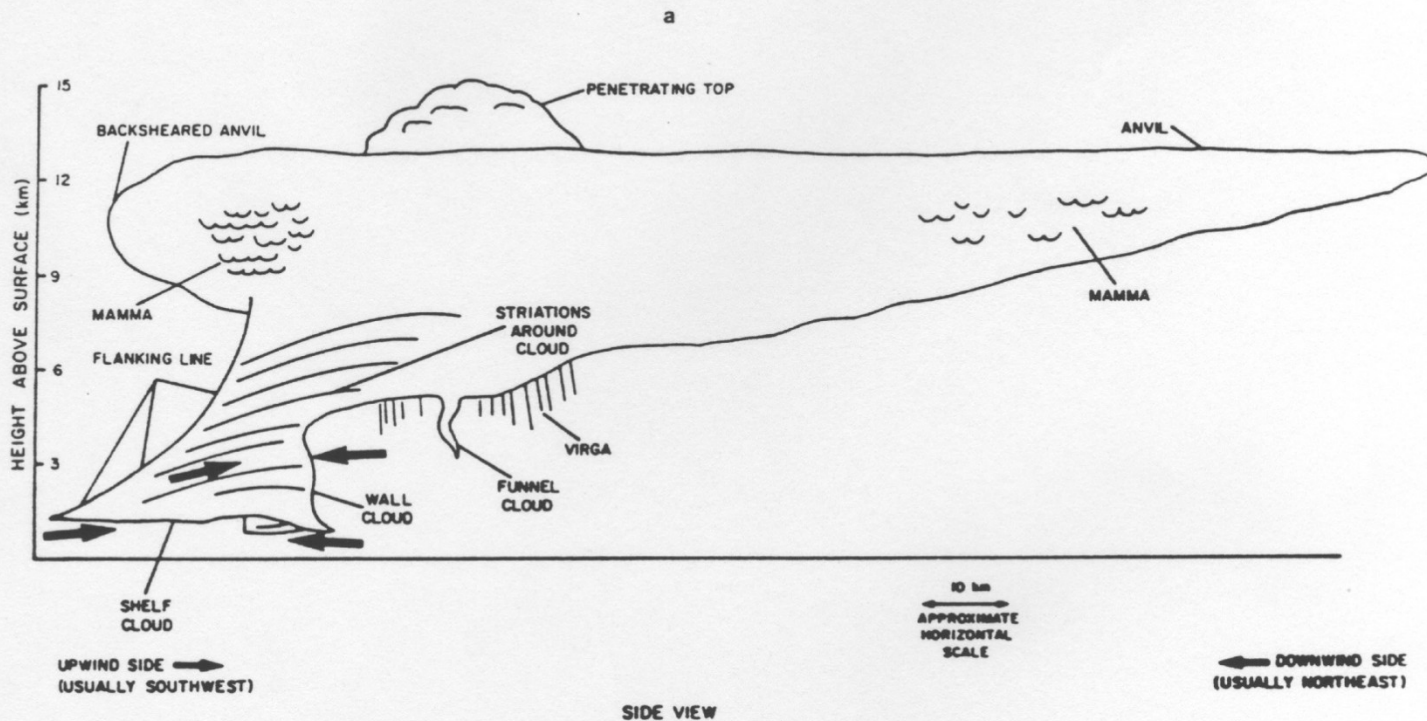
Typical “Tornado Alley” storms



Skeletal "classic" supercell, looking WNW



Low precipitation (LP) Supercell Form more along the dryline in western Great Plains



These require less shear because there is little associated precipitation to produce a cold pool.

Fujita Scale:

Gives a scale for tornado damage



Professor Ted Fujita

Now we use the Enhanced Fujita (EF) scale, which has slightly lower wind speed thresholds for the higher numbers than the original scale.

EF0: Very Weak



Winds: 65-85 mph

Damage: Broken tree branches and signs.

EF1: Weak



Miami, FL

Winds: 86-110 mph

Damage: Small trees snapped and windows broken

EF2: Strong



Winds: 111-135 mph

Damage: Large trees uprooted, weak structures destroyed

EF3: Very Strong



Winds: 136-165 mph

Damage: Severe; trees leveled, cars overturned, walls removed

EF4: Violent



Winds: 166-200 mph

Damage: Major devastation of sturdy structures.

EF5: Catastrophic

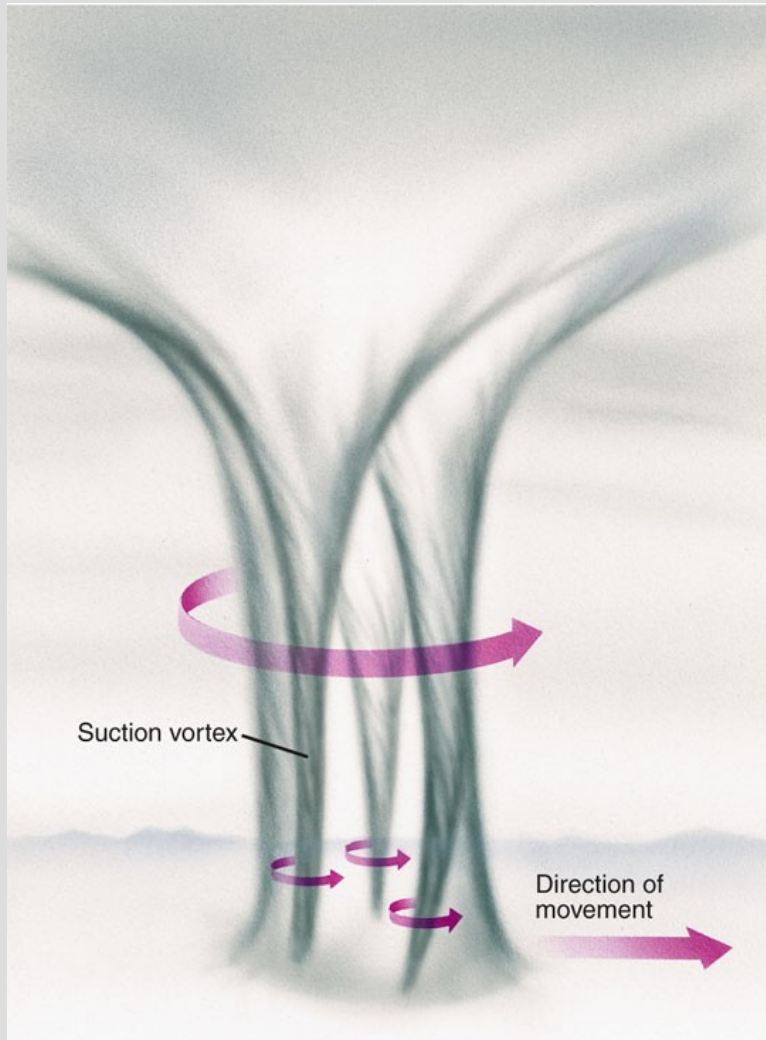


Moore, OK
May 3, 1999

Winds: Over 200 mph

Damage: Ability to move major structures large distances (like houses, trucks, and cars). Total devastation!

Suction Vortices



In the strongest tornadoes, small vortices within the main funnel with even higher wind speeds!

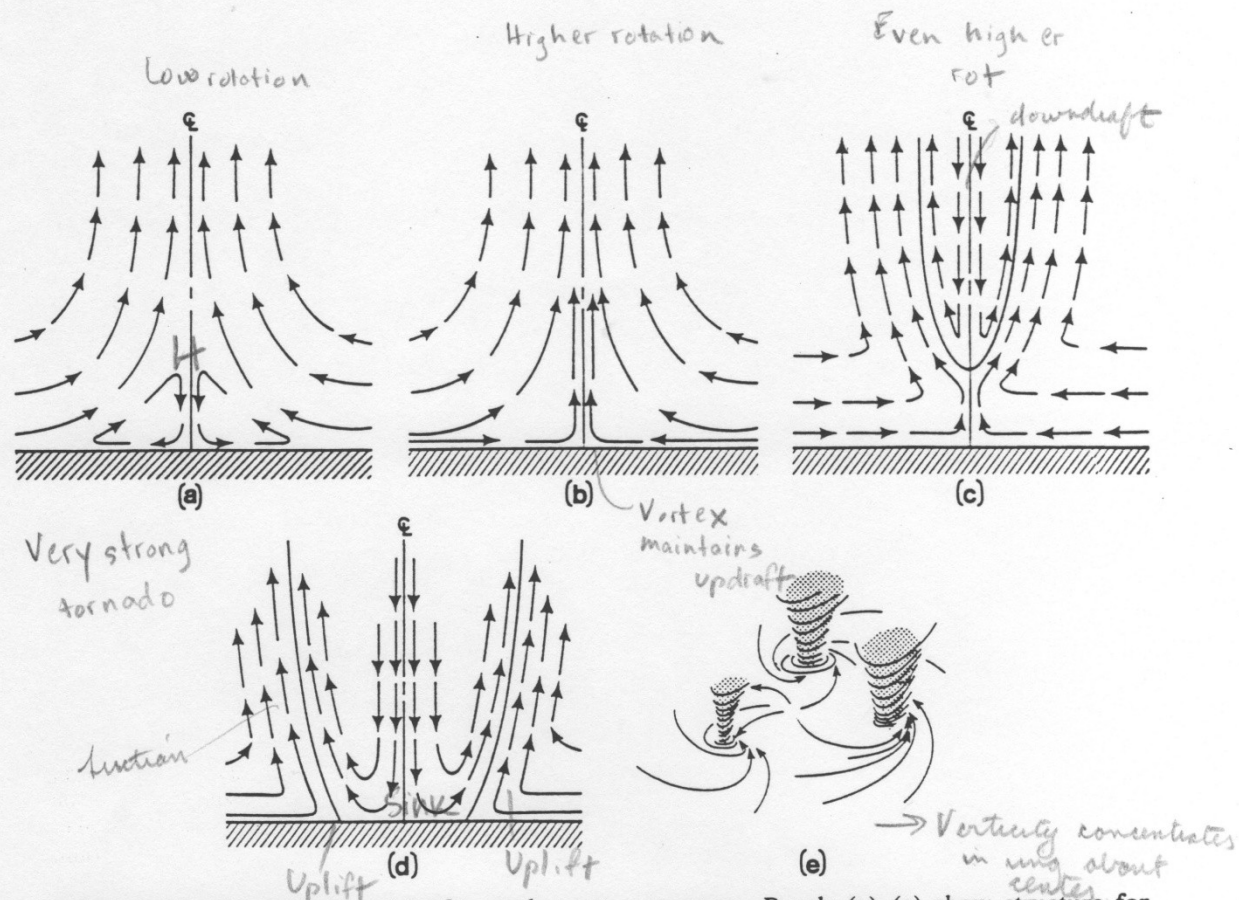
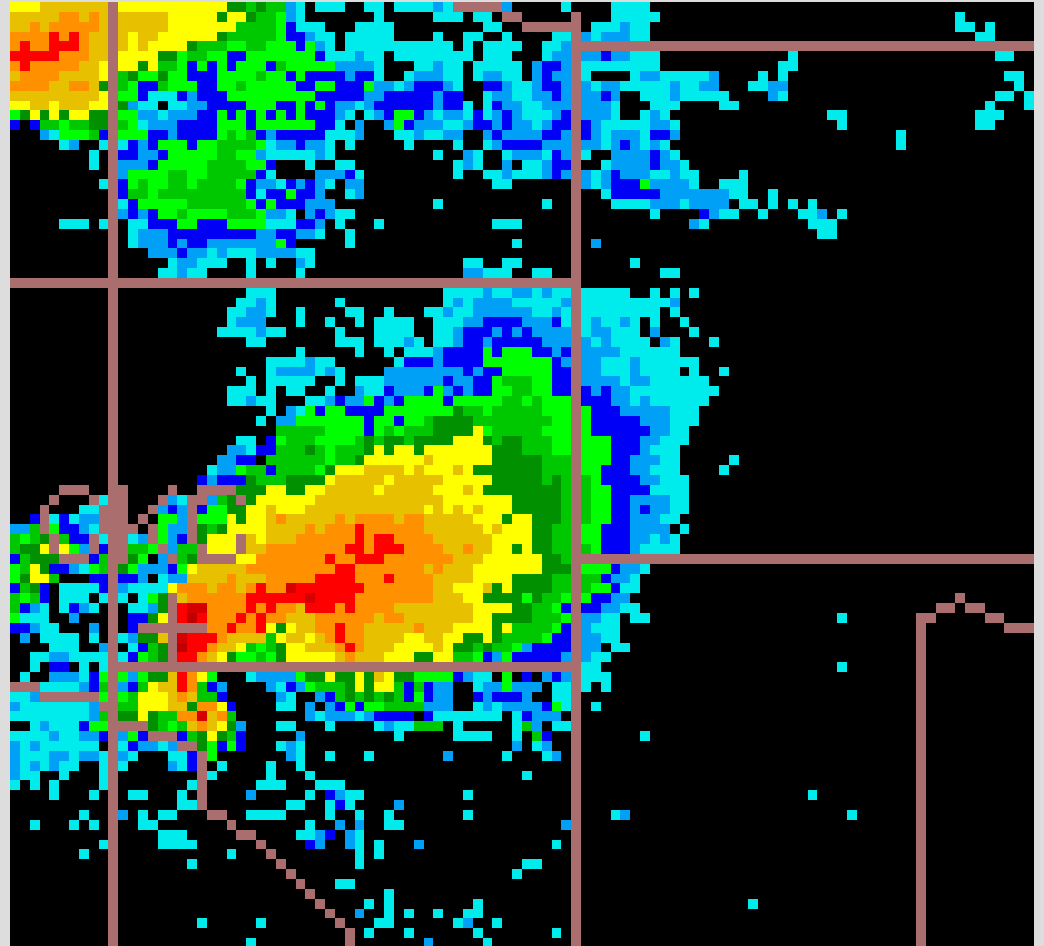


Figure 8.35 Conceptual model of tornado vortex structure. Panels (a)–(e) show structure for successively higher swirl ratio. (a) Weak swirl case: flow in boundary layer separates and passes around corner region. (b) One-cell vortex. (c) Vortex breakdown. (d) Two-cell vortex with downdraft impinging on ground. (e) Multiple vortices. The connected CL indicates the center line. (From Davies-Jones, 1986 and Lewellen, 1976.)

swirl ratio $\propto \frac{V_T}{w}$

RADAR REFLECTIVITY

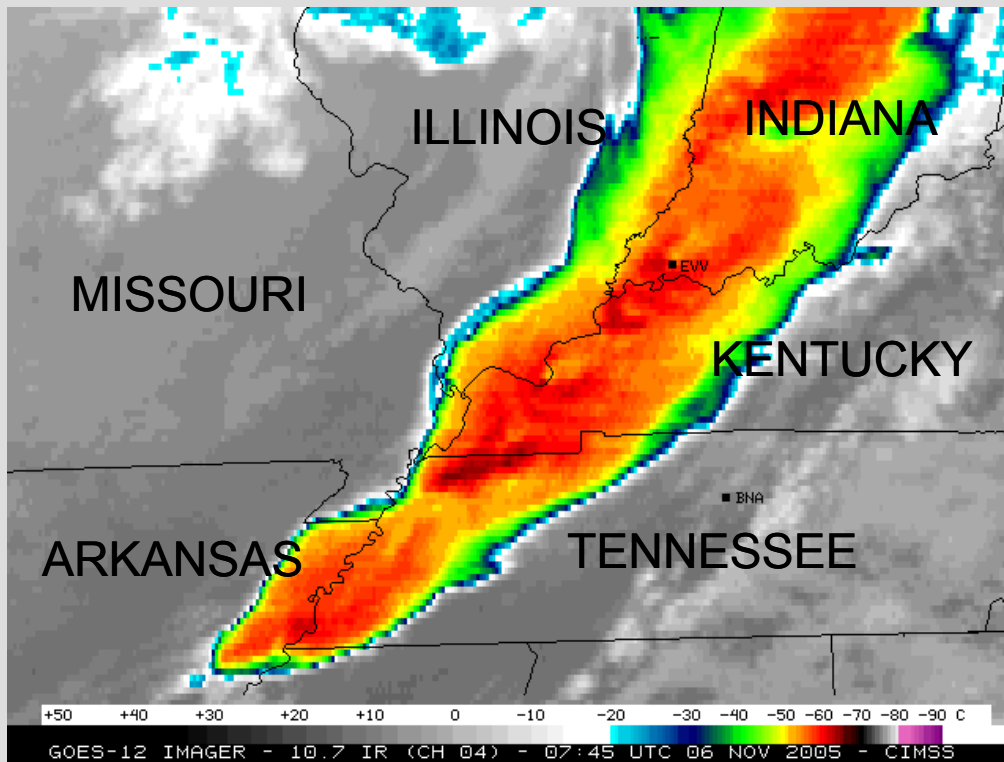
**Moore,
Oklahoma
May 3, 1999**



Meteorological Analysis

Sunday, Nov. 6, 2005

IR SATELLITE IMAGERY



A severe squall line along a cold front was moving through the lower Ohio River Valley.

National Weather Service in Paducah, KY, issued a severe thunderstorm watch.

Squall line broke down into supercell thunderstorms in the early morning hours after midnight.

(CIMMS, U. Wisc.)

Meteorological Analysis

Sunday, Nov. 6, 2005

*EVANSVILLE, INDIANA
RADAR REFLECTIVITY*



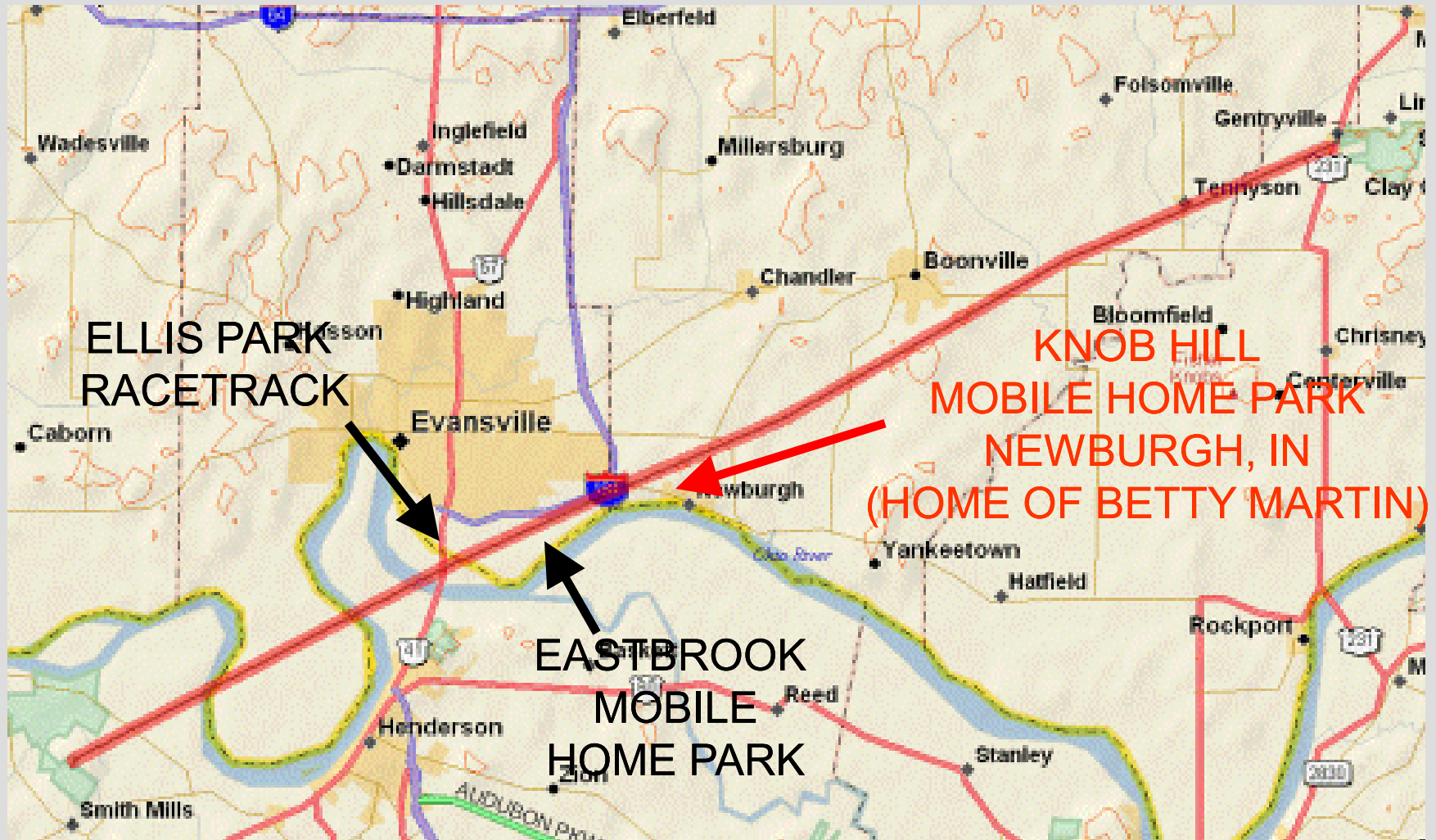
*VIEW FROM DEACONESS HOSPITAL
DOWNTOWN EVANSVILLE*



Before 2 AM, F3 tornado touched down near Smith Mills, Kentucky.

Several minutes later, the storm crossed the Ohio River and headed toward the east side of Evansville, Indiana.

Evansville Tornado Path



Ellis Park Racetrack



Tornado path after Ellis Park



Note the irregular pattern of torn up land—an indicator of the suction vortices within the tornado.

Eastbrook Mobile Home Park



About 20 people died here because of inadequate shelter and the fact the storm hit at 2 AM.

Eastbrook: Arial View of Tornado Path



These residents of this house lived to tell the tale...



Residents of this house in Warrick County, Indiana, survived by seeking shelter in the interior bathroom.

That was the only room left standing!

Greensburg, Kansas Wiped off the map May 4, 2007.



A more detailed and quantitative consideration of organized convection: Part IV

Microbursts

Original notes from Profs. Richard Johnson and Ted Fujita

What is a microburst?

Fujita's definition: a short-lived, strong downdraft with associated outburst of surface winds extending outward 4 km or less and winds as high as 75 m s^{-1}

What they do: Produce damaging surface winds at outflow boundaries. These can become haboobs (dust storms) in Arizona during the monsoon, if the soil is sufficiently dry enough.

Physical cause: sublimation or evaporation of precipitating particles from a convective cloud into dry, unsaturated air below cloud base. The sublimation or evaporation cools the air, causing it to be negatively buoyant relative to the surrounding environment and sink rapidly to the ground.

Wet vs. Dry: Depends on whether there is precipitation that reaches the ground. Wet microbursts, though they precipitate, tend to have more evaporation below cloud base and typically produce stronger winds.



Dry microburst near Denver, CO.



Wet microburst on the west side of Tucson, near Ryan Field



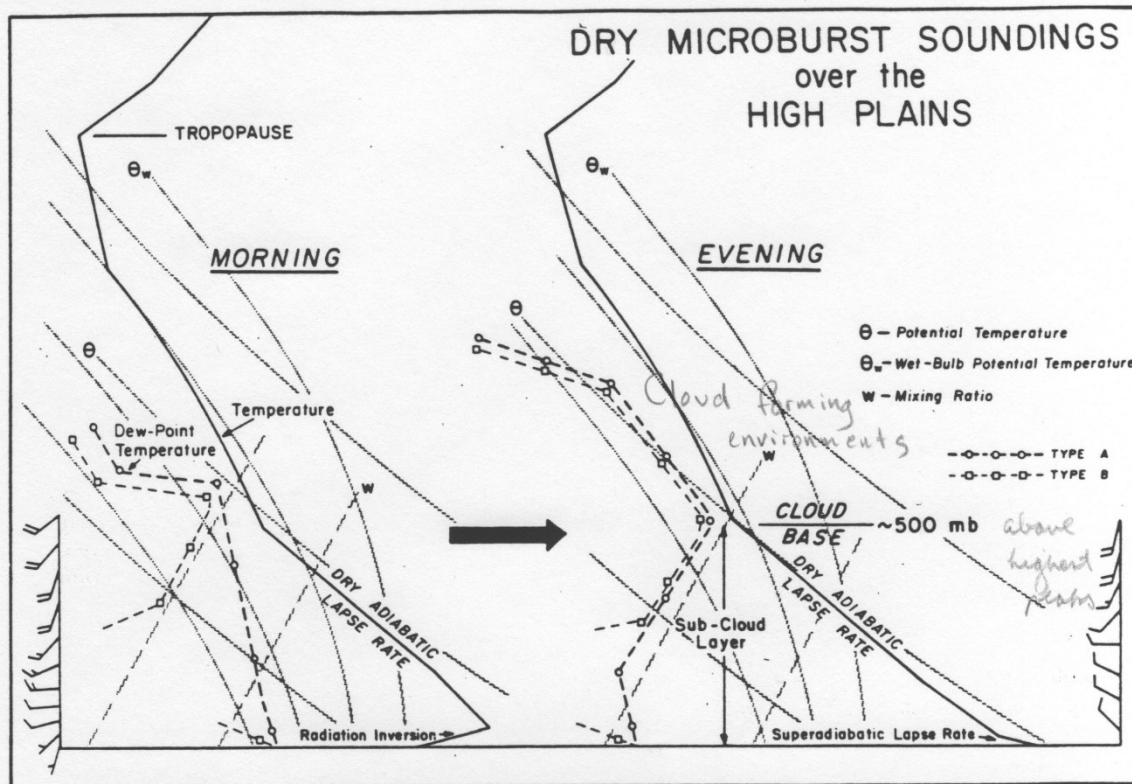


FIG. 8. Model of the characteristics of the morning and evening soundings favorable for dry-microburst activity over the High Plains.

Deep dry adiabatic lapse rate, moist air aloft
 → Result of heating over high terrain

Clouds form over mtns - upslope + lifting, then move out onto plains. Precipitation falls & cools environment

Typical velocities achieved by microbursts can be estimated by considering the vertical momentum equation

$$\frac{dw}{dt} = \frac{\partial w}{\partial t} + \mathbf{v} \cdot \nabla_H w + w \frac{\partial w}{\partial z} = g \frac{T'_v}{T_v}, \quad (1)$$

where $T_v = T(1 + 0.61q - \ell)$ is the virtual potential temperature and ℓ is the hydrometeor mixing ratio. Thus, both sublimative/evaporative cooling and water loading can contribute to a downward acceleration. Assuming steady, horizontally homogeneous conditions, (1) can be integrated from the starting level of the downdraft (z) to the ground ($z = 0$):

$$\int_z^0 \frac{\partial w^2}{\partial z} dz = \int_z^0 g \frac{T'_v}{T_v} dz,$$

or

$$\frac{w^2}{2} = \int_0^z -g \frac{T'_v}{T_v} dz,$$

where w is the speed of a downdraft (starting from rest) when it reaches the ground. If we assume $T'_v/T_v = \text{constant} = \Delta T_v/T_v$, then we can solve for w :

$$w = \sqrt{-2g \frac{\Delta T_v}{T_v} z}. \quad \text{Temp deficit in parcel.}$$

For a $\Delta T_v = -3\text{K}$, $T_v = 300\text{ K}$ and $z = 3\text{ km}$,

$$w \approx \left(\frac{2(10)(3)(3 \times 10^3)}{300} \right)^{1/2} \approx 24 \text{ m s}^{-1}.$$

Thus, a very strong downdraft can be produced from only a modest temperature deficit. The key to its intensity is the great depth of the nearly dry-adiabatic layer – a rather common occurrence in Colorado in the summer. In the case of wet microbursts, a greater amount of precipitation leads to a greater depth of initial descent along a moist adiabat (or nearly so), thus yielding a larger temperature deficit in the downdraft. Therefore, deep dry-adiabatic layers are not needed to produce intense wet microbursts.

Quantitative estimation of downdraft CAPE on Skew-T, log-P diagram

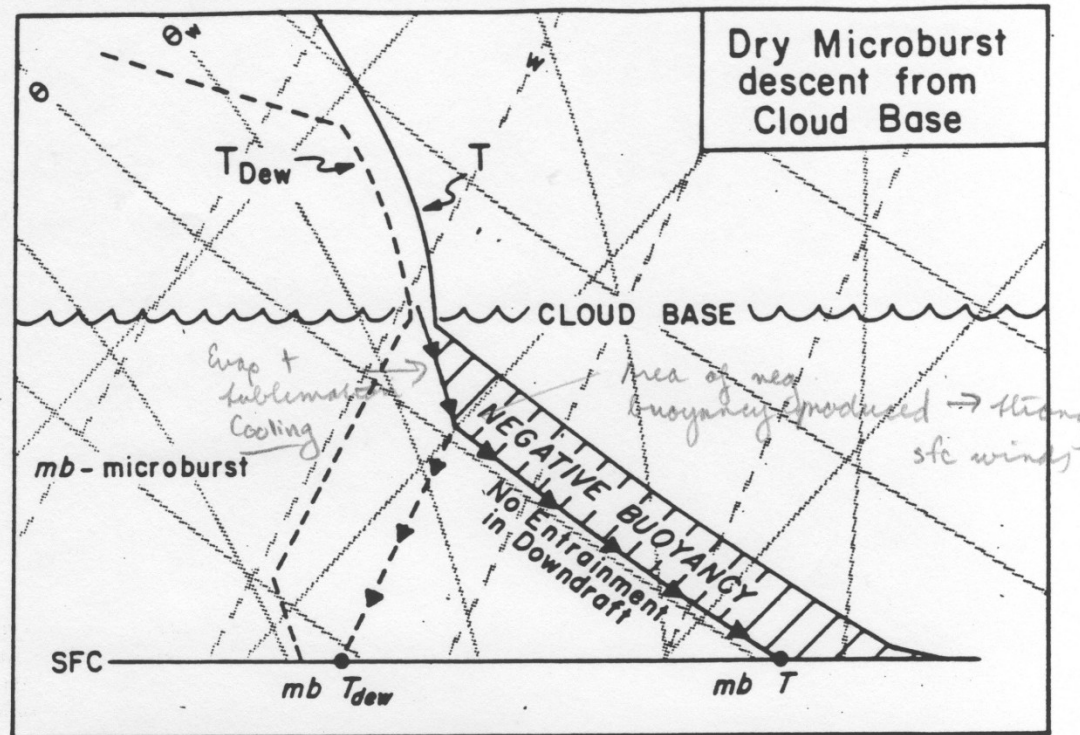
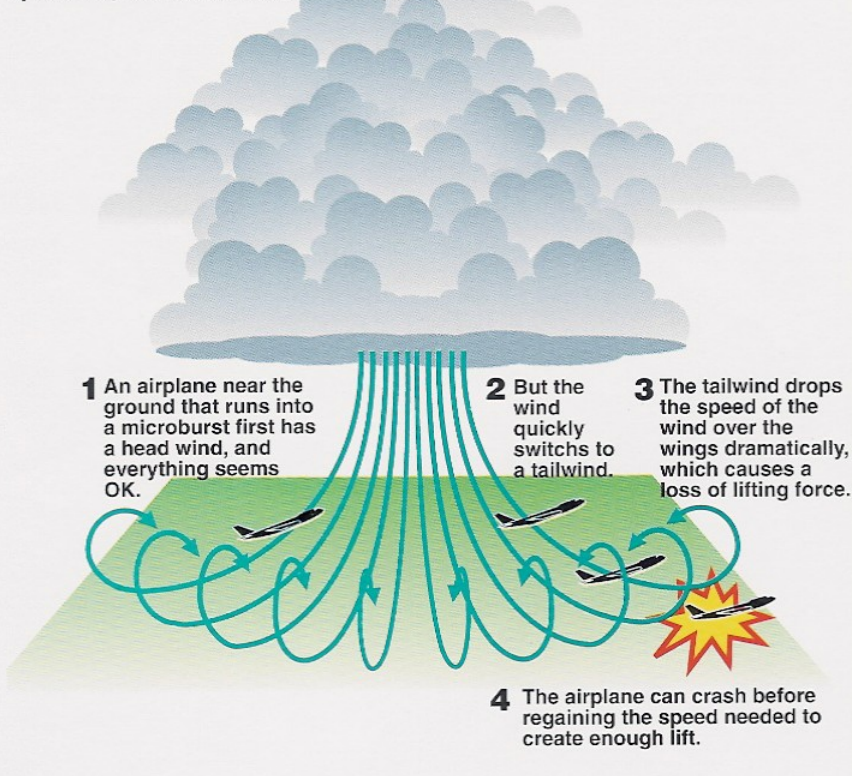


FIG. 10. Model of the thermodynamic descent of a dry microburst from cloud base. Surface temperature and dew-point temperature within the microburst are determined from PAM data. No entrainment into the downdraft is assumed.

Microburst Aviation Hazard

What makes microbursts dangerous

A microburst is just one kind of wind shear — a sudden change in wind speed or direction — but it's dangerous to aircraft close to the ground. As awareness of the danger grew in the 1980s, pilots began receiving special training in avoiding microbursts and in coping with them. The United States government is also installing special airport microburst detection radars.



(Williams)



Delta Flight 191
Crashed August 2, 1985
Cause: Microburst related wind shear and pilot error

Delta airlines crash sounding

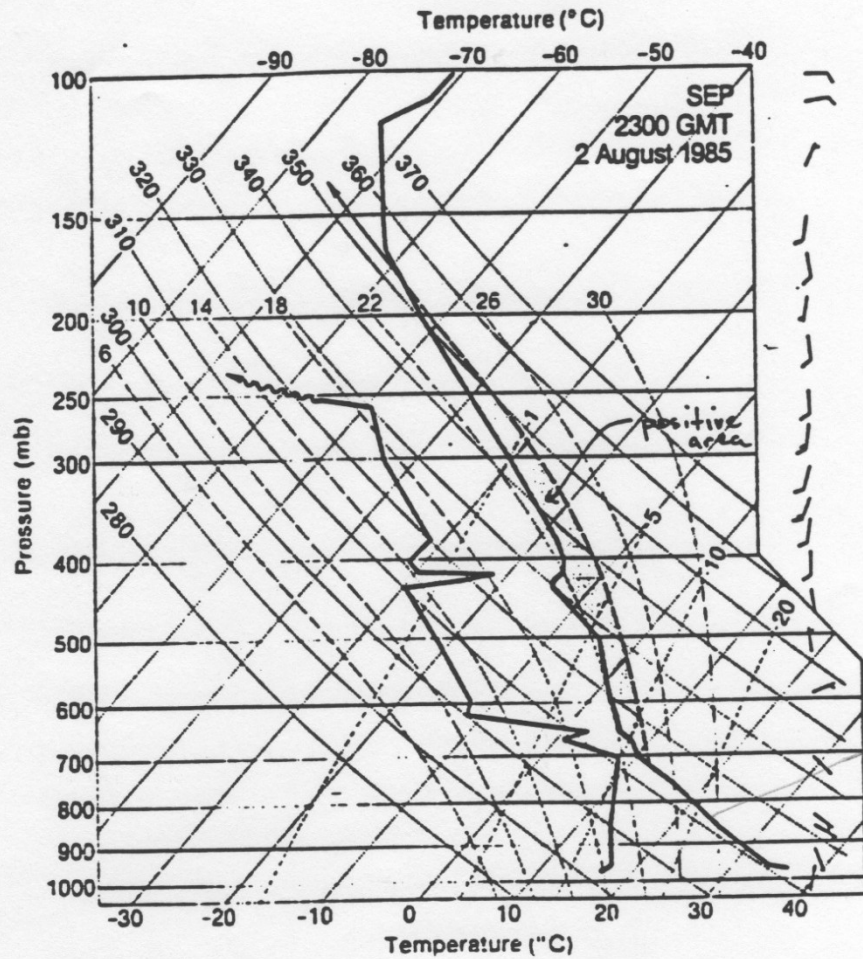
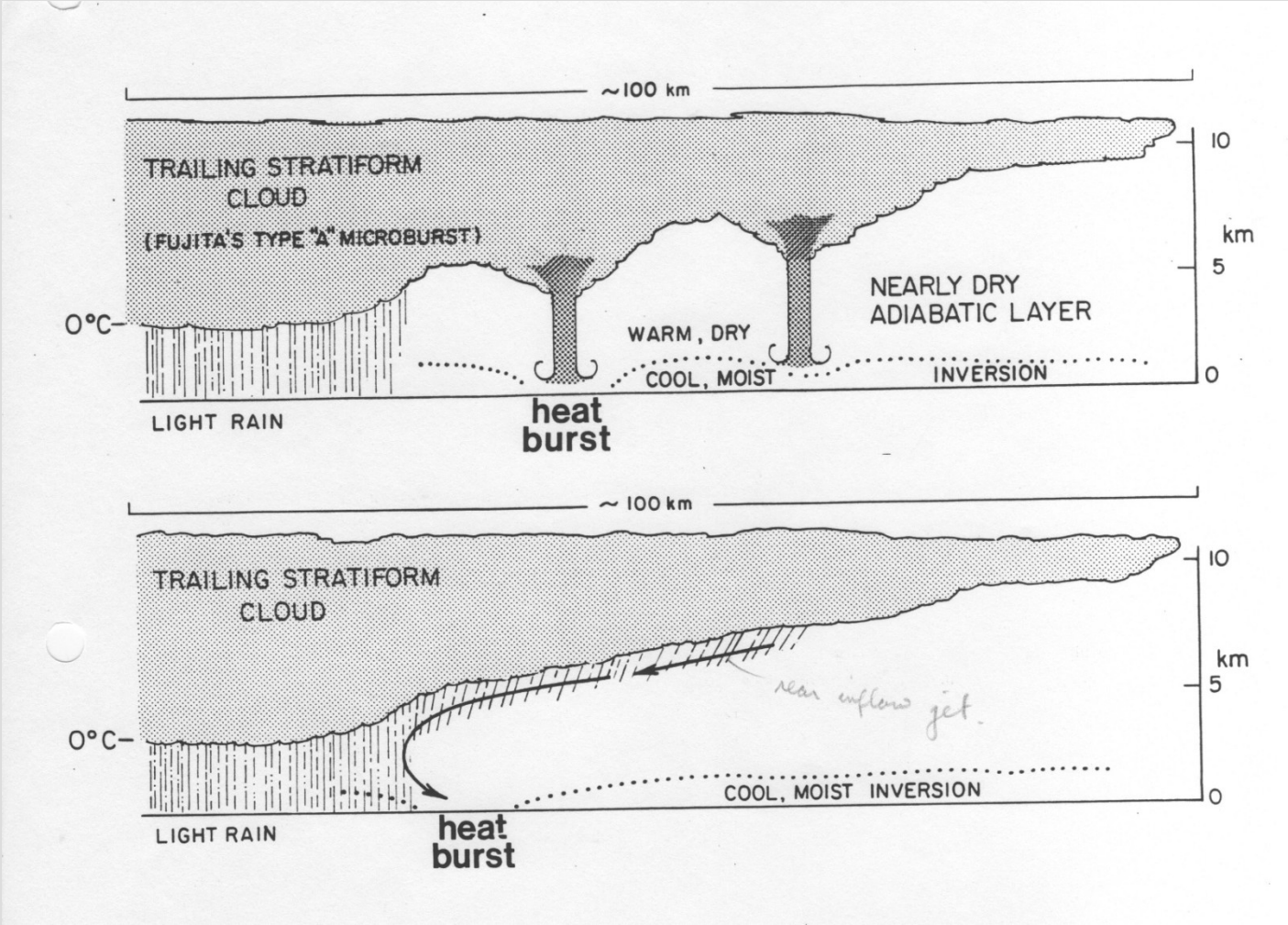
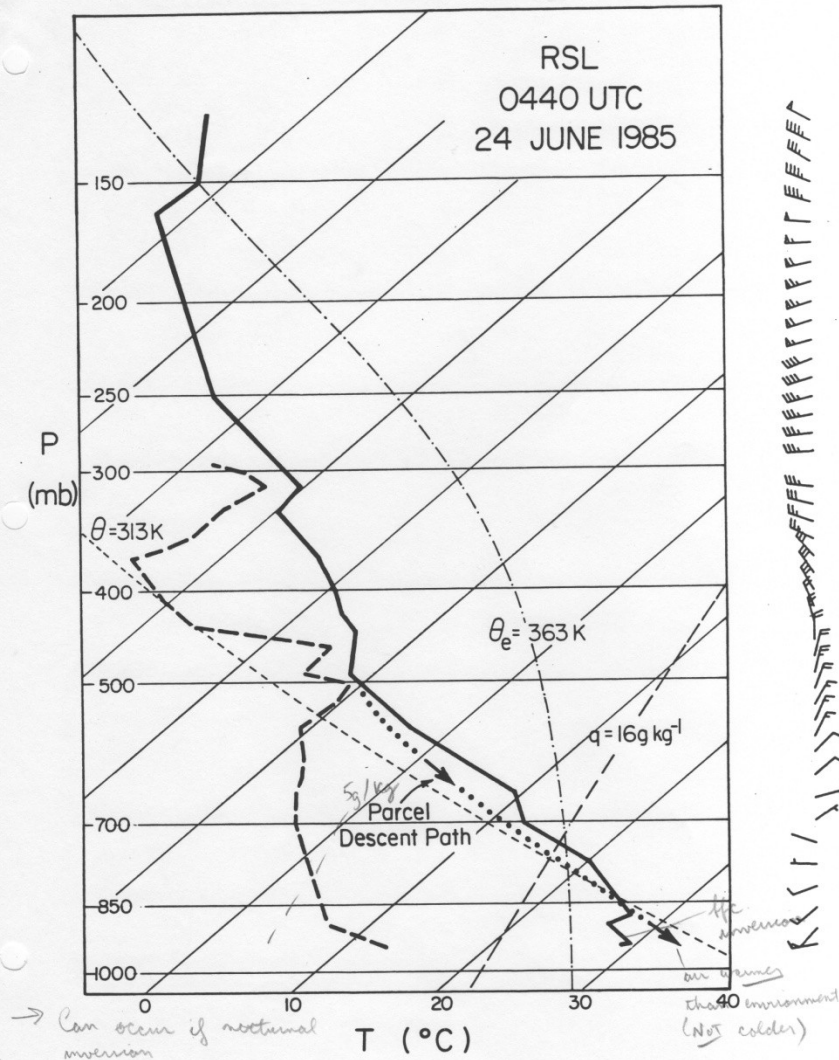


Figure 4. Skew-T/log-P plot of the sounding released at 2300 GMT, 2 August 1985, at Stephenville. Positive area in updraft is shaded red.

Can also get microbursts in association with descending air in the trailing stratiform region





Warm microbursts originating in the trailing stratiform region are characterized by the “onion” sounding.

Typical onion sounding

- Moist aloft
- Dry adiabatic in deep layer below cloud base
- Shallow inversion where air is moist near the ground.